

# Triple Gauge Couplings and Polarization at the ILC

Philip Bechtle, Wolfgang Ehrenfeld, Ivan Marchesini

Deutsches Elektronen-Synchrotron DESY, Notkestraße 85, 22607 Hamburg, Germany

The work presented in this note was developed in the framework of detector R&D and physics studies for the International Linear Collider (ILC), a planned  $e^+e^-$  accelerator that will reach center of mass energies up to 500 GeV in its first stage.

A simultaneous measurement of longitudinal beam polarization and Triple Gauge Couplings (TGCs) at the ILC is implemented, using fully simulated Monte Carlo events. In order to perform such a measurement, semileptonic decays of the  $W$ -pairs at  $\sqrt{s} = 500$  GeV are selected. Additionally, two techniques to measure the polarization alone are also compared.

Assuming 80% longitudinal polarization for the electron beam and 60% for the positron beam, a statistical relative precision of better than 0.2% on the average beam polarization of both beams is achieved at an integrated luminosity of  $250 \text{ fb}^{-1}$ . In the option of a low positron polarization of 30%, with an integrated luminosity of  $500 \text{ fb}^{-1}$  the statistical relative precision on the average polarization is  $\sim 0.1\%$  for the electron beam and  $\sim 0.35\%$  for the positron beam. Three independent TGCs are fitted simultaneously with the polarization, without losing sensitivity on the polarization. An absolute statistical uncertainty on the couplings is reached of the order of  $10^{-3}$ .

## Contents

|          |  |           |
|----------|--|-----------|
| <b>1</b> | <b>Introduction</b>                                | <b>2</b>  |
| <b>2</b> | <b>Triple Gauge Couplings</b>                      | <b>3</b>  |
| <b>3</b> | <b>W-pair Production and Polarization</b>          | <b>7</b>  |
| <b>4</b> | <b>Selection of W-pair Events</b>                  | <b>9</b>  |
| 4.1      | Polarization Configurations . . . . .              | 10        |
| 4.2      | Selection . . . . .                                | 11        |
| <b>5</b> | <b>Measurement of the Polarization</b>             | <b>16</b> |
| 5.1      | The Modified Blondel Scheme . . . . .              | 16        |
| 5.1.1    | Theory . . . . .                                   | 19        |
| 5.1.2    | Application . . . . .                              | 19        |
| 5.2      | The Angular Fit . . . . .                          | 20        |
| 5.2.1    | Templates of $\cos\theta_W$ . . . . .              | 21        |
| 5.2.2    | Performance of the Angular Fit . . . . .           | 22        |
| <b>6</b> | <b>Triple Gauge Couplings and Polarization</b>     | <b>27</b> |
| 6.1      | Simulation of the Triple Gauge Couplings . . . . . | 27        |
| 6.2      | Triple Gauge Couplings Impact . . . . .            | 28        |
| 6.3      | Decay Angles of the W-pair . . . . .               | 29        |
| 6.4      | Simultaneous Fit . . . . .                         | 30        |
| 6.5      | Results . . . . .                                  | 35        |
| <b>7</b> | <b>Systematics</b>                                 | <b>39</b> |
| 7.0.1    | Efficiency . . . . .                               | 39        |
| 7.0.2    | Integrated Luminosity . . . . .                    | 39        |
| 7.0.3    | Assumptions on the Polarization . . . . .          | 42        |
| <b>8</b> | <b>Conclusions</b>                                 | <b>45</b> |

## 1 Introduction

During the last decades experimental evidences of the Standard Model (SM) have been accumulated at several experiments and the SM has come to be regarded as the best description of electromagnetic, weak and strong interactions up to the investigated energies. However, despite the many successes, some shortcomings have been identified and new theories have been formulated to rectify them.

A relevant feature of the SM is the presence of non-Abelian self-couplings between the gauge bosons, that carry the electromagnetic and the weak forces: the  $W$ s, the  $Z$  and the  $\gamma$ . In particular, triple couplings between the gauge bosons in the vertices  $WW\gamma$  and  $WWZ$  occur, as largely experimentally established. A precise measurement of the TGCs not only represents a proof of the SM expectations, but is also a window to eventual new physics not predicted by the SM, contributing to the TGCs through the effect of new particles and couplings via radiative corrections. Should the new physics be not directly accessible at the available center-of-mass energies of ongoing or upcoming experiments, being sensitive to it via deviations from the SM values of the TGCs would be particularly relevant.

The measurement of the TGCs was performed at LEP (Large Electron-Positron collider) and Tevatron experiments. No deviations from the SM were observed, but the limits obtained at these experiments can be significantly improved at future colliders.

Today's most powerful high energy physics project is the proton-proton Large Hadron Collider (LHC) at CERN, where no major improvement on the experimental limits on anomalous couplings in the vertices  $WW\gamma$  and  $WWZ$  is expected. Unprecedented precisions could be achieved at a future lepton collider, such as the International Linear Collider (ILC), a planned  $e^+e^-$  accelerator that will be able to reach center of mass energies up to 500 GeV in its first phase.

One of the unique features of the ILC is the possibility of both electron and positron beam polarization. A longitudinal electron polarization of at least 80% is part of the ILC baseline design in the Reference Design Report (RDR) and the option of a longitudinal positron polarization is also considered. The positron beam produced by the RDR baseline source has a polarization of 30% and beamline space has been reserved for an eventual upgrade up to a polarization of 60%.

The physics program of the ILC highly benefits from having polarized beams. The polarization provides a tool for strongly improving the sensitivity to new physics in SM precision tests, in searches for new particles and for the measurement of the interactions of new physics. For many of these applications, the benefit of the polarization is effective, provided that the systematics from the uncertainty on the beam polarization are brought to a negligible level.

While polarimeters are used to measure the polarization on a bunch-by-bunch basis, the absolute calibration of the average luminosity-weighted polarization at the interaction point (IP) with respect to the measurement of the polarimeters, can only be obtained using a physics process. The  $W$ -pair production can be used to achieve this goal, due to its strong sensitivity to the beam polarization. The  $W$ -pair process is also a golden channel for the measurement of the TGCs, as the LEP experience teaches. Hence, it is possible to combine the two measurements in a global fit of polarization and TGCs. Such a measurement has been implemented using fully-simulated  $W$ -pairs in the International Large Detector (ILD) [1] model for the ILC, at  $\sqrt{s} = 500$  GeV. In order to measure the  $W$  charge with high purity, only semileptonic decays ( $q\bar{q}l\nu$ ) of the  $W$ -pair are selected, where one  $W$  decays

either into an electron or a muon, and the associated neutrino, while the other decays into a quark-antiquark pair.

Two techniques to measure the polarization alone have also been compared: i) the modified Blondel scheme, only relying on the different total cross sections of the  $W^+W^-$  production for different incoming beam polarizations; and ii) the angular fit method, which uses the distribution of the production angle  $\cos\theta_W$  of the  $W^-$  with respect to the  $e^-$  beam axis. When fitting simultaneously the polarization and the TGCs, two angular observables describing the leptonic decay of the  $W$  are also exploited.

## 2 Triple Gauge Couplings

The electromagnetic and the weak interactions are treated together in the SM as a unified gauge theory. The gauge group of the electroweak sector of the SM is:

$$SU(2)_L \otimes U(1)_Y. \quad (1)$$

The  $SU(2)$  gauge transformation acts on left-handed ( $L$ ) weak isospin ( $I$ ) doublets, while the  $U(1)$  gauge theory acts on isospin singlets assigned the hypercharge  $Y$ . The weak hypercharges are chosen to reproduce the observed electric charges, through the connection  $Q = I_3 + \frac{1}{2}Y$ , known as the Gell-Mann-Nishijima formula.

The non-Abelian nature of the  $SU(2)_L$  group results in self-interactions between the gauge bosons. In particular, a TGC term is present in the Lagrangian, that can be expressed as [2]:

$$\begin{aligned} \mathcal{L}_{TGC} &= -\frac{1}{2}g(\partial_\mu W_\nu^i - \partial_\nu W_\mu^i)\varepsilon_{ijk}W^{j\mu}W^{k\nu} \\ &= ig \sin\theta_W(\hat{W}_{\mu\nu}^- W^{+\mu} - \hat{W}_{\mu\nu}^+ W^{-\mu})A^\mu + ig \sin\theta_W \hat{A}_{\mu\nu} W^{-\mu}W^{+\nu} \\ &+ ig \cos\theta_W(\hat{W}_{\mu\nu}^- W^{+\mu} - \hat{W}_{\mu\nu}^+ W^{-\mu})Z^\nu + ig \cos\theta_W \hat{Z}_{\mu\nu} W^{-\mu}W^{+\nu}, \end{aligned} \quad (2)$$

where  $i, j = 1, 2$ ,  $\hat{V}_{\mu\nu} = \partial_\mu V_\nu - \partial_\nu V_\mu$  and  $V_\mu = W_\mu, A_\mu, Z_\mu$ . The first and the second terms describe the  $\gamma WW$  vertex with coupling strengths  $e = g \sin\theta_W$  while the third and the fourth terms describe the  $ZWW$  vertex with coupling strengths  $g \cos\theta_W = e/\tan\theta_W$ .

The TGC term is experimentally well established. Fig. 1 shows the measured cross section of the  $W$ -pair production at LEP [3]. The prediction of the SM agrees perfectly with the data only when the TGC vertices are included. Under different assumptions it would follow a completely wrong trend.

This result represents a notable success of the gauge theory. At the time of the formulation of the SM, the necessity of gauge bosons self-couplings was not driven by experimental observations or theoretical motivations. In fact, the gauge self-couplings are not inserted by hand in the framework, but arise naturally when applying the gauge principle to a non-Abelian symmetry group. Only afterward it has been experimentally confirmed that this feature is actually realized in nature.

New physics not predicted by the SM would contribute to the TGCs through the effect of new particles and couplings via radiative corrections. A general, model independent and phenomenological approach to physics beyond the SM is given by the effective Lagrangian [5]. In this approach, the SM is considered as an effective sub theory, providing a low energy approximation of a Grand Theory (GT). The GT would manifest itself at low energies

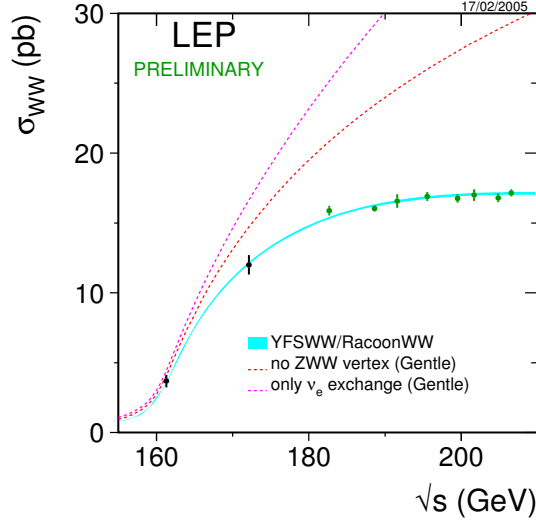


Figure 1: The dependence of  $\sigma_{WW}$  on  $\sqrt{s}$  as measured at LEP. The error bars include statistical and systematic contributions. The lower dashed curve shows the cross section that would be expected if the  $WWZ$  couplings were zero, while the upper dashed curve refers to the case where both the  $WWZ$  and the  $WW\gamma$  vertices are excluded. The continuous curve shows the SM expectations with all the TGC vertices included. From [4].

through small deviations from the SM, which can be described by an effective Lagrangian, having a purely phenomenological meaning. The effective Lagrangian parametrizes in a model-independent way, i.e. in the most general way, the effects of the GT at low energies.

The effective Lagrangian for the TGCs in the vertices  $WW\gamma$  and  $WWZ$  is given by [6]:

$$\begin{aligned}
i\mathcal{L}_{eff}^{WWV} &= g_{WWV} \left[ g_1^V V^\mu (W_{\mu\nu}^- W^{+\nu} - W_{\mu\nu}^+ W^{-\nu}) + \kappa_V W_\mu^+ W_\nu^- V^{\mu\nu} + \right. \\
&\quad \frac{\lambda_V}{m_W^2} V^{\mu\nu} W_\nu^{+\rho} W_{\rho\mu}^- + i g_5^V \varepsilon_{\mu\nu\rho\sigma} ((\partial^\rho W^{-\mu}) W^{+\nu} - W^{-\mu} (\partial^\rho W^{+\nu})) V^\sigma \\
&\quad \left. + i g_4^V W_\mu^- W_\nu^+ (\partial^\mu V^\nu + \partial^\nu V^\mu) - \frac{\tilde{\kappa}_V}{2} W_\mu^- W_\nu^+ \varepsilon^{\mu\nu\rho\sigma} V_{\rho\sigma} - \right. \\
&\quad \left. \frac{\tilde{\lambda}_V}{2m_W^2} W_{\rho\mu}^- W^{+\mu} \varepsilon^{\nu\rho\alpha\beta} V_{\alpha\beta} \right], \tag{3}
\end{aligned}$$

where  $V \equiv \gamma$  or  $Z$ , the overall couplings are defined as  $g_{WW\gamma} = e$  and  $g_{WWZ} = e \cot \theta_W$  and  $\epsilon^{0123} = 1$ . Equation 3 gives the most general Lorentz invariant  $WWV$  vertex. It introduces fourteen complex parameters, i.e. 28 real couplings. In the SM, at tree level, the non-null couplings are  $g_1^Z = g_1^\gamma = \kappa_Z = \kappa_\gamma = 1$ , while all other couplings are vanishing. Electromagnetic gauge invariance fixes  $g_1^\gamma = 1$  and  $g_5^\gamma = 0$ , when considering on-shell photons.  $g_1^V$ ,  $\kappa_V$  and  $\lambda_V$  conserve  $C$  and  $P$  separately, while  $g_5^V$  violates  $C$  and  $P$  but conserves  $CP$ . Finally,  $g_4^V$ ,  $\tilde{\kappa}_V$  and  $\tilde{\lambda}_V$  parameterize a possible  $CP$ -violation in the bosonic sector [6].

The couplings can be related to physical properties of the gauge bosons. The charge  $Q_W$ , the magnetic dipole moment  $\mu_W$  and the electric quadrupole moment  $q_W$  of the  $W^+$

| Decay Mode       | BR   | averaged $\epsilon$ |
|------------------|------|---------------------|
| qqqq             | 45 % | 85 %                |
| $\mu\nu$ qq      | 15 % | 80 %                |
| $e\nu$ qq        | 15 % | 80 %                |
| $\tau\nu$ qq     | 15 % | 60 %                |
| $\ell\nu\ell\nu$ | 10 % | 65 %                |

Table 1:  $WW$  decay modes with relative branching ratios  $BR$  and average selection efficiencies  $\epsilon$  at the LEP experiments. From [4].

can be related to the  $C$ - and  $P$ -conserving couplings [7]:

$$Q_W = eg_1^\gamma, \quad \mu_W = \frac{e}{2m_W} (g_1^\gamma + \kappa_\gamma + \lambda_\gamma), \quad q_W = -\frac{e}{m_W^2} (\kappa_\gamma - \lambda_\gamma). \quad (4)$$

So far, the best limits on the TGCs have been obtained at LEP [8]. The couplings have been experimentally tested using the  $e^+e^- \rightarrow W^+W^-$  process. The angular distributions of the  $W$ -pair are more sensitive to the TGCs than the inclusive measurement, based on the total cross section. The differential  $W$ -pair cross sections with respect to 5 angles are considered:

- the angle  $\theta_W$  between the  $W^-$  and the  $e^-$  beam;
- the polar and azimuthal angles of the fermion in the decay  $W^- \rightarrow f\bar{f}$  calculated in the rest frame of the  $W^-$ ;
- the corresponding polar and azimuthal angles of the fermion in the decay of the  $W^+$ .

All the possible  $WW$  decays, summarized in Tab. 1 together with the branching ratios and the corresponding average selection efficiencies, are taken into account for the final combined results of the LEP experiments [8]. In addition, also the single- $W$  [9, 10] ( $e^+e^- \rightarrow W^\mp e^\pm \nu(\bar{\nu})$ ) and the single- $\gamma$  [11, 12] ( $e^+e^- \rightarrow \gamma \bar{\nu}_e \nu_e$ ) productions are exploited, being sensitive to the  $WW\gamma$  vertex.

Some assumptions are made to reduce the number of free parameters in Eq. 3. Assuming  $C$  and  $P$  conservation the 14 complex couplings are reduced to 6 real couplings:  $g_1^\gamma$ ,  $g_1^Z$ ,  $k_\gamma$ ,  $k_Z$ ,  $\lambda_\gamma$  and  $\lambda_Z$ .  $g_1^\gamma$  is fixed by requiring electromagnetic gauge invariance. The requirement of local  $SU(2)_L \times U(1)_Y$  gauge invariance introduces the further constraints [13]:

$$\begin{aligned} \Delta k_Z &= -\Delta k_\gamma \tan^2 \theta_W + \Delta g_1^Z \\ \lambda_\gamma &= \lambda_Z, \end{aligned} \quad (5)$$

with  $\Delta$  indicating the deviation from the SM tree-level value and  $\theta_W$  the electroweak mixing angle. One is then left with three independent real couplings:  $g_1^Z$ ,  $k_\gamma$  and  $\lambda_\gamma$ .

Fits to these three TGCs are performed with methods where only one parameter is allowed to vary and the other two are fixed to their SM prediction. The constraints obtained combining the results from the LEP experiments are shown in Fig. 2. No significant deviations from the SM are found, within a few percent precision.

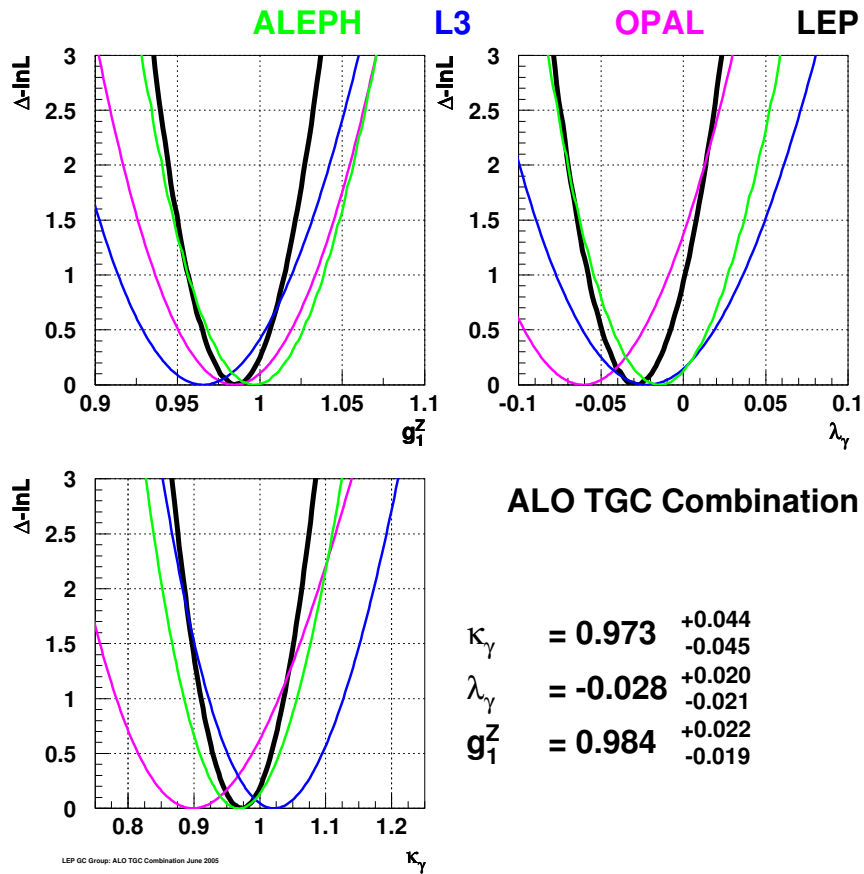


Figure 2: Fit results on the TGCs at LEP. The likelihood fits for  $g_1^Z$ ,  $\kappa_\gamma$  and  $\lambda_\gamma$  from single-parameter fits are shown for the different experiments separately (thin colored curves) and for the combined results (thick black curve). The uncertainties indicate the 68% C.L. limits from the combined results. From [8].

The ALEPH experiment at LEP also performed a fit to all 14 complex couplings, relaxing all the constraints on  $C$  and  $P$  conservation and on electromagnetic and  $SU(2)_L \times U(1)_Y$  gauge invariance [14]. Out of all the 28 real parameters one at the time was allowed to vary, while the others were fixed to the SM predictions. The results of this test for the already considered couplings do not show significant deviations from the SM:

$$\begin{aligned} \text{Re}(g_1^Z) &= 1.066 \pm 0.076 \\ \text{Re}(k_\gamma) &= 1.071 \pm 0.061 \\ \text{Re}(\lambda_\gamma) &= 0.096 \pm 0.066. \end{aligned} \tag{6}$$

The same is true for all the remaining couplings.

The Tevatron experiments have confirmed the results obtained at LEP, without improving the precision [15, 16]. While the LHC will excel in the measurement of the neutral  $ZZZ$  and  $ZZ\gamma$  couplings, which are not discussed in this note, the foreseen experimental uncertainties on the TGCs is at the  $10^{-2}$  level and is not expected to improve significantly the current limits [17]. A breakthrough can be made at the future ILC, where it is possible to gain one order of magnitude in the uncertainty on the TGCs, reaching a sensitivity of the order of  $10^{-3}$ , as shown in the following.

### 3 W-pair Production and Polarization

Indicating with  $N_R$  ( $N_L$ ) the number of beam particles with definite right-handed (left-handed) helicity  $\lambda = +\frac{1}{2}$  ( $\lambda = -\frac{1}{2}$ ), the longitudinal polarization of the beam is defined as:

$$\frac{N_R - N_L}{N_R + N_L}. \tag{7}$$

Since the beam particles can be regarded as being massless, the helicity corresponds to their chirality.

The beam polarization will maximize the physics potential of the ILC, both in the performance of precision tests and measurements of the SM, and also in revealing the properties of new physics beyond the SM, such as Supersymmetry. The most general benefit given by having polarized beams is the increase in available statistics and hence a reduction of the statistical errors. In many studies the beam polarization allows to enhance the signal, while suppressing background contributions. This is particularly important for searches of new physics, for which the signal rates are expected to be extremely small compared to the SM background. Furthermore, it should be noted that the beam polarization is essential to address several important studies, such as the measurement of the chiral quantum numbers of new particles. For a complete treatment of the topic we refer the interested reader to reference [18], which also underlines the importance of having both the beams polarized. In fact, a high electron polarization alone does not replace the essential contribution of having a polarized positron beam in addition.

With longitudinally-polarized beams one can distinguish between two different cases, depending on the production diagrams:

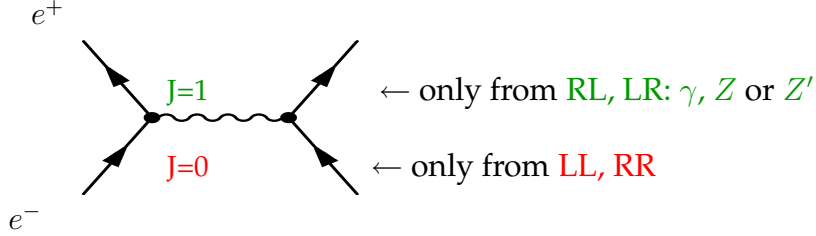


Figure 3: Possible configurations in  $s$ -channel diagrams: the helicities of the incoming  $e^+e^-$  beams are directly coupled. Within the SM only the recombination into a vector particle with  $J = 1$  is possible, which is given by the LR (Left-handed electron, Right-handed positron) and RL configurations. New physics models might contribute to  $J = 1$  but also to  $J = 0$ , hence the LL or RR configurations. From [18].

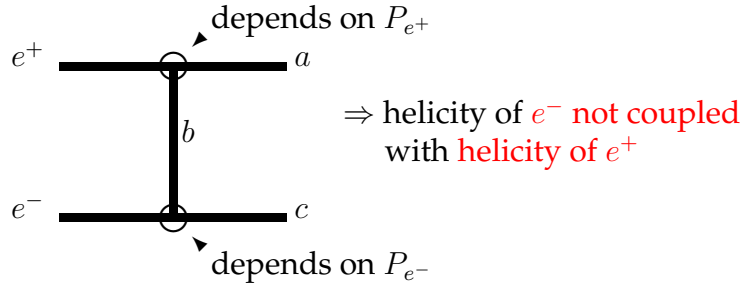


Figure 4: Possible configurations in  $t$ - and  $u$ -channel diagrams: the helicity of the incoming beam is directly coupled to the helicity of the final particle and is completely independent from the helicity of the second incoming particle. From [18].

- in annihilation diagrams, as shown in Fig. 3, the helicities of the incoming beams are coupled to each other. In the SM they need to be opposite from one another in order to recombine into the vector boson mediator, the  $Z$  or the  $\gamma$ , since only in this way they can add up to give  $J = 1$ . This might not be true in case of new physics. Some models allow  $s$ -channel diagrams to be mediated by a scalar particle.
- in exchange diagrams, as shown in Fig. 4, the helicities of the incoming beams are directly coupled to the helicities of the final particles. In this case all helicity configurations for the beams are in principle possible, although some constraints might be given by the allowed couplings between the beam particles and the produced ones.

In Fig. 5 the leading tree-level Feynman diagrams for the  $W^+W^-$  production are shown. In the two  $s$ -channel diagrams (center and right) the incoming  $e^+$  and  $e^-$  annihilate to give the vector boson mediator. As explained above, in the SM only the recombination into a vector particle with  $J = 1$  is possible, i.e. the beams have to carry opposite helicities. This constraint is no longer valid for the  $t$ -channel diagram (left). Since  $W$ -bosons can only

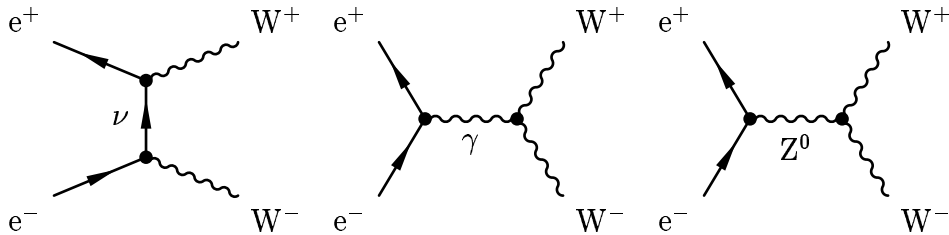


Figure 5: *Leading tree-level Feynman diagrams for the  $W^+W^-$  production. On the left the  $t$ -channel with  $\nu$  exchange, in the center and on the right the two  $s$ -channels with  $\gamma$  or  $Z^0$  exchange.*

couple to left-handed electrons and right-handed positrons, this channel is suppressed for the polarization configuration with right-handed electrons and left-handed positrons and also in the case of same helicity beams. As a consequence of this behavior, the total cross section for the  $W$ -pair is strongly sensitive to the polarization, as shown in Fig. 6. The visible peak in the distribution, corresponding to left-handed electrons and right-handed positrons, is due to the  $t$ -channel enhancement for such polarizations.

The  $t$ - and the  $s$ -channel not only have a different dependence on the polarization, but also generate a different topology of the  $W$ -pair, since the  $t$ -channel production is more boosted in the forward region.

These features make the  $W$ -pair production a perfect candidate for the measurement of the luminosity-weighted polarization. In addition, the large cross section has statistical benefits. Since the results obtained at LEP show that the  $W$ -pair production is an excellent channel also for the measurement of the TGCs (Sec. 2), this channel is suitable for a simultaneous measurement of polarization and TGCs, as shown below.

The present study is only concerned with longitudinal polarization. For completeness, it should be mentioned that the physics program at the ILC would benefit also from transversely-polarized beams [18]. In particular, although longitudinally-polarized beams are sufficient to measure most TGCs, in the most general case, where a non-null imaginary part is also allowed, the transverse polarization is necessary in order to be sensitive to the imaginary parts of some couplings. However, in the here presented work we make the same assumptions on the couplings used in the LEP combined results (Sec. 2) and only real TGCs are considered.

## 4 Selection of $W$ -pair Events

The present analysis relies on Monte Carlo events fully simulated using the ILD detector model and includes the complete SM background. A center of mass energy of 500 GeV and an 80% longitudinally-polarized electron beam are assumed and two options are considered for the longitudinal polarization of the positron beam: a high polarization of 60% and a low polarization of 30%. The final results are reported for an integrated luminosity of  $500 \text{ fb}^{-1}$ , but propagations of the uncertainties at different luminosities are also shown.

This section illustrates how Monte Carlo samples for different polarizations are created and describes in detail the selection applied in order to separate the signal from the background.

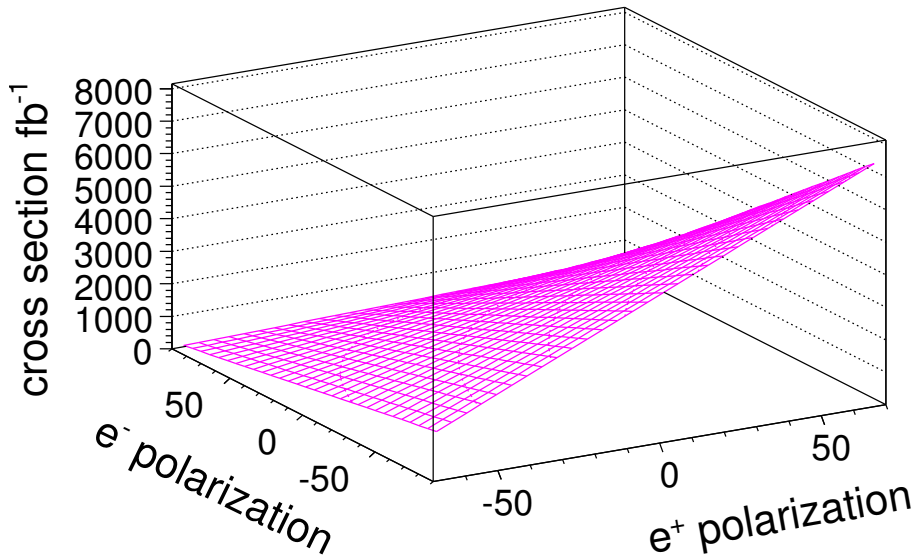


Figure 6: Total cross section of the selected semi-semileptonic decay channels of the  $W$ -pairs (Sec. 4.2) as a function of the electron and positron beam polarizations, at  $\sqrt{s} = 500$  GeV.

#### 4.1 Polarization Configurations

The Monte Carlo events are generated for 100%-polarized beams. Events from different files, corresponding to different polarization configurations, need to be properly mixed in order to obtain realistic cases of partial polarizations  $P_{e^+}$  and  $P_{e^-}$ . The number of events generated with a polarization of  $P(e^+, e^-) = (\pm 100\%, \pm 100\%)$  to be used is given by:

$$N_{\pm\pm}^{events} = \sigma_{\pm\pm} \cdot \mathcal{L} \cdot w_{\pm\pm}(P_{e^+}, P_{e^-}), \quad (8)$$

where  $\sigma_{\pm\pm}$  is the cross section of the considered process,  $\mathcal{L}$  is the desired luminosity and the necessary weight  $w_{\pm\pm}(P_{e^+}, P_{e^-})$  is derived directly from the properties of the polarization:

$$\begin{aligned} P &= P_R - P_L \\ P_R + P_L &= 100. \end{aligned} \quad (9)$$

Here,  $P$  is the beam polarization and  $P_R$  ( $P_L$ ) is the percentage of right-handed (left-handed) events. For example, a +60% positron polarization is obtained mixing 80% events with right-handed positron beam with 20% events with left-handed positron beam. Analogously, -80% electron polarization equals 10% right-handed and 90% left-handed electron beam. Combining the two requests, to get +60% positron and -80% electron polarization, one needs:

$$\begin{aligned}
weight_{++}(+60, -80) &= 80\% \cdot 10\% = 0.08, \\
weight_{+-}(+60, -80) &= 80\% \cdot 90\% = 0.72, \\
weight_{-+}(+60, -80) &= 20\% \cdot 10\% = 0.02, \\
weight_{--}(+60, -80) &= 20\% \cdot 90\% = 0.18.
\end{aligned}
\tag{10}$$

This example can be generalized, obtaining the weight  $w_{\pm\pm}(P_{e^+}, P_{e^-})$  for any other desired polarization set. It should be noted that not all the four  $\sigma_{\pm\pm}$  are necessarily non-null. For example, for all processes occurring exclusively via  $s$ -channel only events with  $P(e^+, e^-) = (+100\%, -100\%)$  and  $P(e^+, e^-) = (-100\%, +100\%)$  are available.

## 4.2 Selection

Due to the favorable reconstruction of the angular distributions only semileptonic decays ( $q\bar{q}l\nu$ ) of the  $W$ -pair have been selected, where one  $W$ -boson decays either into an electron or a muon, and its associated neutrino, while the other decays into a quark-antiquark pair. The angular distribution of the  $W$ -pair is expressed by the  $\cos\theta_W$  variable, where  $\theta_W$  is the angle of the  $W^-$  with respect to the  $e^-$  beam axis. The charge of the lepton tags the charges of the two  $W$ -bosons. Since the  $W$ -pair is emitted back-to-back, one can always reconstruct the  $\theta_W$  angle together with the  $W$ -boson invariant mass from the hadronically decaying  $W$ -boson, using the four-momenta of the two jets produced in the decay. The same information could be obtained, in principle, also from the leptonic decaying  $W$ -boson, using the reconstructed lepton four-momentum and the missing four-momentum due to the neutrino, but a lower precision would be achieved in this case (cf. Fig. 11).

The semileptonic decay in which the leptonic decaying  $W$ -boson decays into a tau and the associated neutrino has been excluded, since this signal has a larger background and the determination of the charge of the lepton is less reliable, resulting from the possibility of the candidate tau being formed from tracks from the fragmentation of the quarks. Additionally, multiple neutrinos might be present in the final state due to the decay of the tau. This channel is labeled in the following as *tau-signal* and is considered as background.

The other two excluded decay channels of the  $W$ -pair are the fully leptonic decay ( $l\nu l\nu$ ), in which each  $W$ -boson decays into a lepton and its associated neutrino, and the fully hadronic decay ( $q\bar{q}q\bar{q}$ ), in which each  $W$ -boson decays into two quarks. The fully hadronic decay has not been selected, since the charge of the  $W$ -boson cannot be reconstructed with sufficient precision from the jets of the hadronic decay. Moreover, a combinatoric background is introduced, due to the different possible ways of combining the four jets of the decays into two  $W$ -bosons. The fully leptonic decay is excluded as well, due to the lower cross section and selection efficiency. The reconstruction of this channel is also disturbed by the presence of multiple neutrinos in the final state. The different features, which characterize the selection of the different decay channels of the  $W$ -pair, are fully described in the LEP literature, see e.g. [19].

The selection has been optimized for a Monte Carlo sample of  $20\text{ fb}^{-1}$  and the results obtained have been propagated to higher luminosities. The entire SM background has been taken into account. The complete four- and six-fermion,  $q\bar{q}$ ,  $\gamma\gamma$  and  $Z$ -Strahlung background is included, where the  $\gamma\gamma$  processes are given by the interaction between two radiated or Beamstrahlung photons, while the  $Z$ -Strahlung events are produced by the scattering of a

| Process        | Events      | %      | Weight |
|----------------|-------------|--------|--------|
| Signal         | 107233      | 0.071  | 1.00   |
| Tau-Signal     | 52926       | 0.035  | 1.00   |
| q $\bar{q}$    | 390727      | 0.258  | 1.00   |
| 4 Fermions     | 431247      | 0.285  | 1.00   |
| 6 Fermions     | 20808       | 0.014  | 1.00   |
| $\gamma\gamma$ | 1.50439e+08 | 99.338 | 179.98 |

Table 2: Number of initial signal and background events before the selection. The numbers refer to a positron polarization of +30% and an electron polarization of -80%, at a luminosity of  $20 \text{ fb}^{-1}$ . The average weight applied to compensate for those processes, for which  $20 \text{ fb}^{-1}$  of statistics were not available, is also reported.

photon on a beam electron or positron. In the following these two backgrounds are grouped together under the label  $\gamma\gamma$ .

Not all processes were simulated with sufficient statistics. During the massive ILD Monte Carlo production smaller luminosities were simulated for those processes with a very high cross section and of relatively low importance for most of the physics analysis, most notably the  $\gamma\gamma$ -background. Therefore, the events for these processes need to be given a weight greater than 1 to compensate the low number of events available. However, the  $\gamma\gamma$  is a minor and non-dangerous background for the selected final state and the need of a higher weight does not represent a significant statistical limitation.

Tab. 2 shows the initial amount of background and signal events, before any selection. The numbers refer to a positron polarization of +30% and an electron polarization of -80% for an integrated luminosity of  $20 \text{ fb}^{-1}$ . The same configuration was also chosen for all the figures and tables appearing in this section.

As a preselection of semileptonic  $W$ -pair decays, the following criteria, illustrated in Fig. 7, are applied:

- track multiplicity  $\geq 10$ ;
- center of mass energy  $\sqrt{s} > 100 \text{ GeV}$ ;
- total transverse momentum  $P_T > 5 \text{ GeV}$ ;
- total energy  $E_{SUM} < 500 \text{ GeV}$ ;

The first two requirements mainly constrain the  $\gamma\gamma$  and the  $q\bar{q}$  SM background, the third and fourth account for the expected missing momentum, due to the neutrino.

The DURHAM jet finder algorithm [20] is applied, forcing the event into three jets: one jet is associated to the lepton and two jets are generated by the quarks produced in the hadronic decay of the  $W$ -boson. The jet with the lowest number of particles is identified with the lepton. Clearly, it is not a jet in the physical sense of a compact cascade of particles, but as a distinct object identified using the jet finder algorithm. The lepton could have been isolated, in principle, also employing a specific lepton-finder software, but such an algorithm was not available in the ILCSoft framework at the time this analysis was developed. However, since the lepton tends to occupy a different spacial region, with respect to the jets from the hadronic decay, the jet finder identifies it easily as a separate object. This procedure results

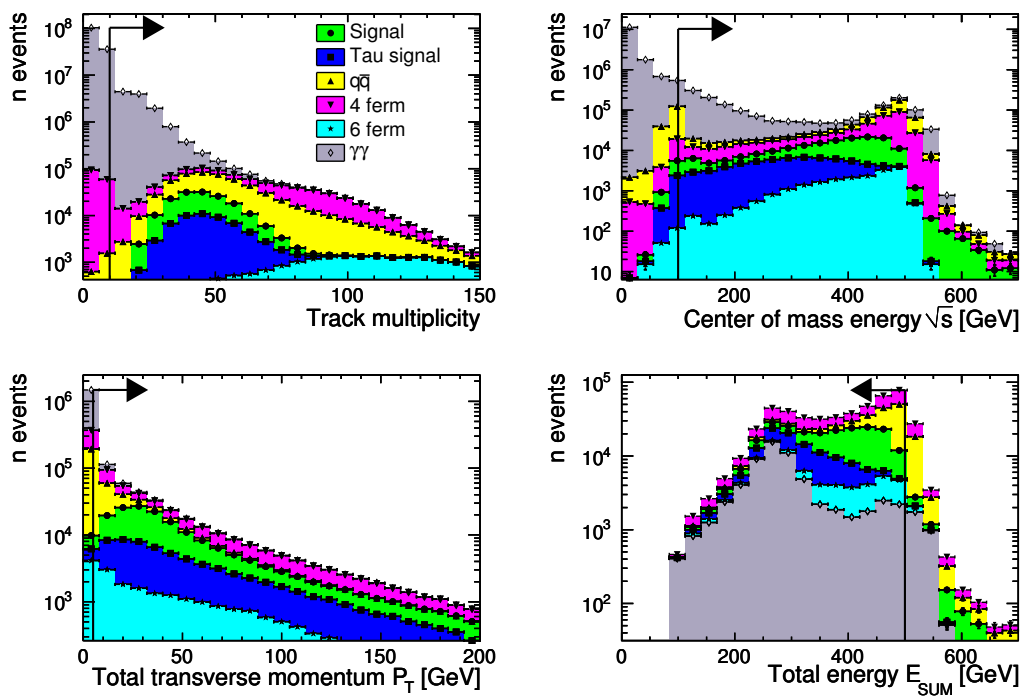


Figure 7: Variables used in the preselection of  $W$ -pairs. The actual cut values are indicated by the lines and the accepted regions by the arrows. Top left: track multiplicity. Top right: center of mass energy  $\sqrt{s}$ . Bottom left: total transverse momentum  $P_T$ . Bottom right: total energy  $E_{SUM}$ .

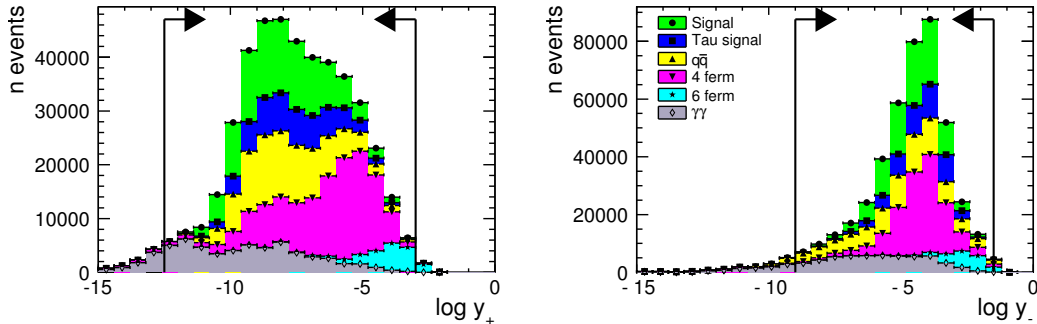


Figure 8: *Logarithm of the  $y_+$  (left) and  $y_-$  (right) variables of the jet finder algorithm. The actual cut values are indicated by the lines and the accepted regions by the arrows.*

in the correct assignment and the proper charge reconstruction of the lepton in about 92% of the cases. An additional criterion is applied to the  $y_+$  and  $y_-$  variables of the jet finder, where the logarithm of the  $y_+$  ( $y_-$ ) variable is accepted in the range  $[-12, -3]$  ( $[-9, -1.5]$ ). The  $y$  variables and the accepted ranges are shown in Fig. 8.

The jet associated with the lepton is required to have at least one track with energy  $> 10$  GeV and to be isolated from the other two jets. The separation is expressed by means of the following angular selection:

$$\begin{aligned}
 (\phi_{\text{lep}} - \phi_{\text{had}}) < \pi &\rightarrow \Delta\Omega_{\text{iso}} = \sqrt{(\theta_{\text{lep}} - \theta_{\text{had}})^2 + (\phi_{\text{lep}} - \phi_{\text{had}})^2} > 0.5, \\
 (\phi_{\text{lep}} - \phi_{\text{had}}) \geq \pi &\rightarrow \Delta\Omega_{\text{iso}} = \sqrt{(\theta_{\text{lep}} - \theta_{\text{had}})^2 + (2\pi - |\phi_{\text{lep}} - \phi_{\text{had}}|)^2} > 0.5. \quad (11)
 \end{aligned}$$

where  $\theta_{\text{lep}}$  and  $\phi_{\text{lep}}$  are the polar and the azimuthal angles of the jet associated with the lepton, while  $\theta_{\text{had}}$  and  $\phi_{\text{had}}$  are the polar and the azimuthal angles of one of the two jets produced in the hadronic decay of the  $W$ -boson, respectively (the same request is repeated for both jets). The isolation variable  $\Delta\Omega_{\text{iso}}$  is shown in Fig. 9 (left).

The suppression of the tau-signal is performed using the following discriminating variable:

$$\tau_{\text{discr}} = \left( \frac{2E_{\text{lep}}}{\sqrt{s}} \right)^2 + \left( \frac{m_W^{\text{lep}}}{m_W^{\text{true}}} \right)^2 < 1, \quad (12)$$

where  $E_{\text{lep}}$  is the reconstructed lepton energy,  $m_W^{\text{lep}}$  is the  $W$ -boson mass as reconstructed from the leptonic decay and  $m_W^{\text{true}}$  is the nominal mass of the  $W$ -boson. Candidates for which  $\tau_{\text{discr}} < 1$  are considered tau-signal events and rejected. Figure 9 (right) shows the discriminating variable.

In order to better reconstruct the missing momentum and consequently the  $W$ -boson leptonic decay, a simple calculation is done to correct for ISR photons lost along the beam pipe without being measured by the forward calorimeters. The four-momentum conservation leads to the following equations containing the missing momentum of the neutrino, the missing momentum of the lost ISR photons and the total measured momentum:

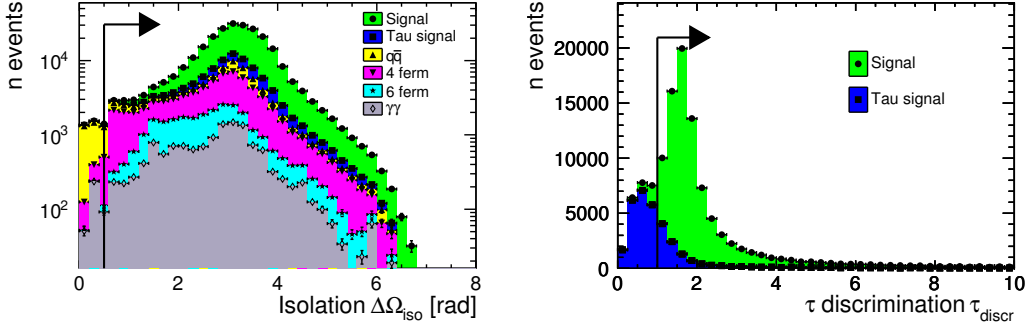


Figure 9: Left: isolation of the jet associated to the lepton from the other two jets, produced in the hadronic decay of the  $W$ -boson. The isolation is expressed by means of the  $\Delta\Omega_{iso}$  variable defined in Eq. 11. Right: discriminating variable  $\tau_{discr}$  used to suppress the contribution of those  $W$ -pair semileptonic events, in which one  $W$ -boson decays into a tau and the associated neutrino. The definition of the variable is given in Eq. 12. The semileptonic  $W$ -boson decays into electrons and muons (signal) are shown in green, while those involving taus (tau-signal) are shown in blue. The discrimination is performed requiring  $\tau_{discr} > 1$ .

$$\begin{aligned}
P_x + P_{\nu,x} &= 0, \\
P_y + P_{\nu,y} &= 0, \\
P_z + P_{\nu,z} + P_\gamma &= 0, \\
E_\nu &= \sqrt{P_{\nu,x}^2 + P_{\nu,y}^2 + P_{\nu,z}^2}, \\
E_\gamma^2 &= P_\gamma^2, \\
E + E_\nu + E_\gamma &= 500,
\end{aligned} \tag{13}$$

where  $P_x, P_y, P_z$  are the components of the total measured momentum,  $E$  is the total measured energy,  $P_\nu$  and  $E_\nu$  are the neutrino missing momentum and energy,  $P_\gamma$  and  $E_\gamma$  are the photon momentum and energy. The indices  $x$  and  $y$  indicate the transverse coordinates (perpendicular to the beam axis), while  $z$  denotes the direction along the beam axis. The photon is assumed to have negligible transverse momentum components ( $x, y$ ), since it is assumed to be lost in the beam pipe.

These equations give two possible solutions for the photon energy:

$$\begin{aligned}
E_\gamma &= \frac{(500 - E)^2 - P_x^2 - P_y^2 - P_z^2}{1000 - 2E - 2P_z}, \\
E_\gamma &= \frac{(500 - E)^2 - P_x^2 - P_y^2 - P_z^2}{1000 - 2E + 2P_z},
\end{aligned} \tag{14}$$

and, therefore, two different momenta for the neutrino. For each set of solutions the  $W$ -boson invariant mass is calculated from the invariant mass of the lepton and the reconstructed missing energy of the neutrino. The solution giving a  $W$ -boson invariant mass

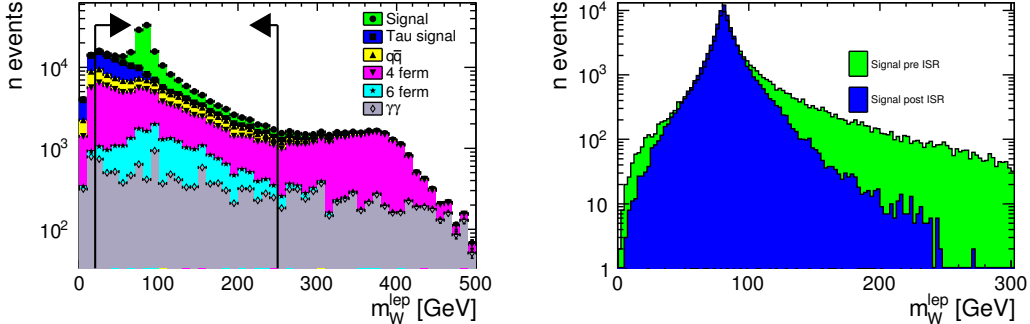


Figure 10: *Left: the selection criteria on the invariant mass of the leptonically-decaying  $W$ -boson ( $m_W^{\text{lep}}$ ) is applied before the ISR correction. The invariant mass  $m_W^{\text{lep}}$  is accepted in the range  $[20,250]$  GeV. Right: measured  $m_W^{\text{lep}}$  distribution before (green) and after (blue) the ISR correction.*

closer to its nominal value is chosen. The benefit of the ISR correction on the reconstruction of  $m_W^{\text{lep}}$  is shown in Fig. 10 (right).

As a consequence of the ISR correction, the invariant mass of the jet associated with the lepton and the missing momentum might be artificially shifted closer to the nominal mass of the  $W$ -boson for some backgrounds. This might cause a selection requirement on the measured  $m_W^{\text{lep}}$  to be less effective in terms of background rejection. In order to minimize this side effect,  $m_W^{\text{lep}}$  is accepted only in the range  $[20,250]$  GeV before applying the ISR correction, as shown in Fig. 10.

After the ISR correction, both  $m_W^{\text{had}}$  (the invariant mass of the products of the  $W$ -boson hadronic decay) and  $m_W^{\text{lep}}$  are required to be in the range  $[40,120]$  GeV. Both  $W$ -boson invariant masses,  $m_W^{\text{had}}$  and  $m_W^{\text{lep}}$ , together with their resolutions are shown in Fig. 11.

Finally, the angular requirement  $\cos\theta_W > -0.95$  is applied, as shown in Fig. 12 (left). The resolution obtained in the reconstruction of  $\cos\theta_W$  is shown in Fig. 12 (right).

The details of the selection are summarized in Tab. 3. The full Monte Carlo sample is sorted in the six groups defined above: signal, tau-signal,  $q\bar{q}$ , four- and six-fermions and  $\gamma\gamma$ . The final efficiency of the selection is about 67%. The selected events include 10% tau-signal events and only 6% of other backgrounds.

## 5 Measurement of the Polarization

In this section two techniques to measure the beam polarization are considered, while the additional measurement of the TGCs is introduced in the next section. The systematic uncertainty that anomalous values of the TGCs would introduce on the measurement of the polarization is calculated in Sec. 6.2.

### 5.1 The Modified Blondel Scheme

The first method considered is a modified Blondel scheme [21]. The original Blondel scheme was intended for processes of electron positron annihilation into two fermions and proposed

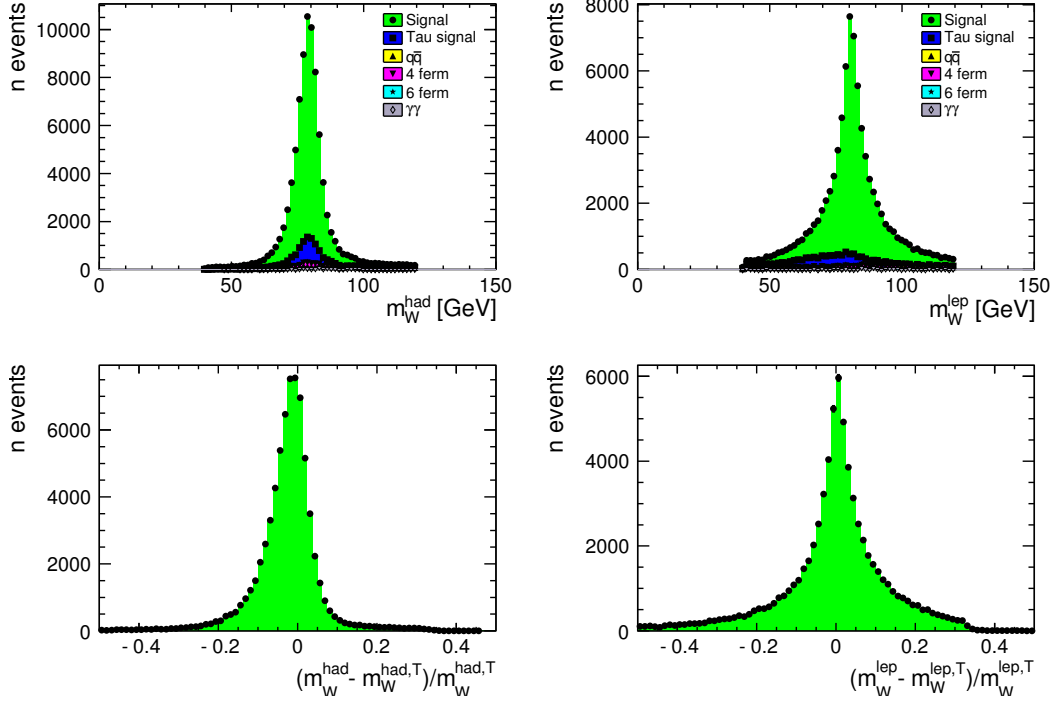


Figure 11: Mass of the  $W$ -boson as reconstructed from the hadronic decay  $m_W^{\text{had}}$  (top left) and from the leptonic decay  $m_W^{\text{lep}}$  (top right). The two bottom distributions show the respective resolutions with  $m_W^{\text{had,T}}$  and  $m_W^{\text{lep,T}}$  indicating the true invariant masses from Monte Carlo simulations.

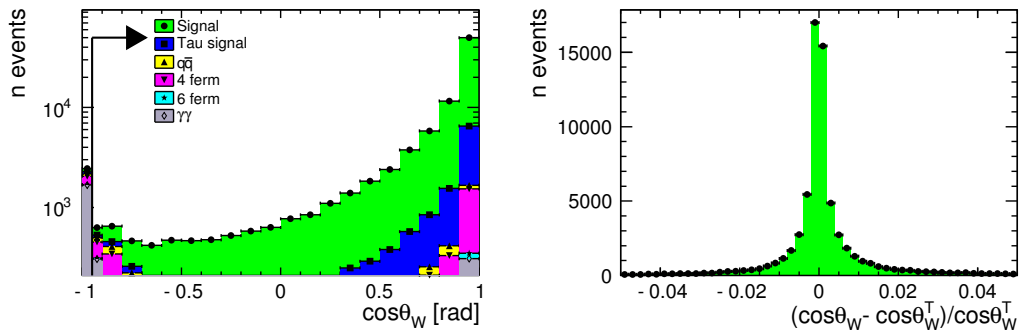


Figure 12: Left: the angular distribution  $\cos\theta_W$ , with the applied requirement  $\cos\theta_W > -0.95$ . Right: resolution of  $\cos\theta_W$ , with  $\cos\theta_W^{\text{T}}$  indicating the true value from Monte Carlo simulations.

| Cut                           | Signal               | Tau-Signal           | q $\bar{q}$             | 4 Fermions            | 6 Fermions            | $\gamma\gamma$                    |
|-------------------------------|----------------------|----------------------|-------------------------|-----------------------|-----------------------|-----------------------------------|
| Initial events                | 107233               | 52926                | 390727                  | 431247                | 20808                 | 1.50439e+08                       |
| n tracks > 10                 | 107229               | 52925                | 389290                  | 290297                | 20663                 | 1.50306e+07                       |
| $\sqrt{s} > 100$ GeV          | 105050               | 51384                | 255396                  | 275494                | 20532                 | 1.14302e+06                       |
| $P_T > 5$ GeV                 | 103681               | 50539                | 109917                  | 139264                | 18185                 | 64510.6                           |
| $E_{SUM} < 500$ GeV           | 102259               | 50502                | 87326                   | 126275                | 17604                 | 61484.6                           |
| $y$ cuts                      | 101882               | 50394                | 84292                   | 122163                | 15714                 | 43260.6                           |
| lepton                        | 84443                | 39166                | 31720                   | 76241                 | 13415                 | 16223.9                           |
| $20 < m_W^{\text{lep}} < 250$ | 82149                | 31951                | 26361                   | 52364                 | 12955                 | 9712.53                           |
| tau selection                 | 79423                | 11226                | 16236                   | 30726                 | 9943                  | 7061.11                           |
| charge lepton                 | 78830                | 10123                | 8720                    | 21934                 | 6636                  | 6775.07                           |
| isolation                     | 78730                | 10050                | 6016                    | 21569                 | 6625                  | 6472.16                           |
| $40 < m_W^{\text{lep}} < 120$ | 75204                | 8936                 | 4308                    | 14100                 | 4351                  | 3890.29                           |
| $40 < m_W^{\text{had}} < 120$ | 71776                | 8422                 | 972                     | 2915                  | 267                   | 2862.12                           |
| $\cos\theta_W > -0.95$        | 71611                | 8287                 | 875                     | 2548                  | 256                   | 1188.53                           |
| Final events                  | 71611                | 8287                 | 875                     | 2548                  | 256                   | 1188.53                           |
| Efficiency                    | $(66.78 \pm 0.14)\%$ | $(15.66 \pm 0.16)\%$ | $(0.2240 \pm 0.0076)\%$ | $(0.591 \pm 0.011)\%$ | $(1.230 \pm 0.076)\%$ | $(7.90 \pm 0.23) \cdot 10^{-4}\%$ |

Table 3: Detailed cut flow of the selection. The full Monte Carlo sample is sorted in six groups: signal, tau-signal, q $\bar{q}$ , four- and six-fermion SM background and  $\gamma\gamma$ . The event numbers refer to a positron polarization of +30% and an electron polarization of -80% for an integrated luminosity of 20 fb $^{-1}$ .

to collect some data also with unpolarized beams. Contrary to this, a similar method is here applied to the  $W$ -pair production, which has also a  $t$ -channel component and, in addition, the altered method does not require data collection with unpolarized beams. Hence, it is called *modified* Blondel scheme.

### 5.1.1 Theory

This technique requires to spend some luminosity on all the four possible combinations of the polarization of the beams:  $++$ ,  $+-$ ,  $-+$  and  $--$ , where the first and the second sign are respectively the sign of the polarization of the positron and of the electron beam. Moreover, the absolute polarization values of the left- and right-handed degrees of beam polarization are required to be equal. Polarization measurements with dedicated polarimeters are needed to measure possible deviations. The beam polarization is then obtained by measuring the total cross section for each helicity configuration [22]:

$$|P_{e^\pm}| = \sqrt{\frac{(\sigma_{-+} + \sigma_{+-} - \sigma_{--} - \sigma_{++})(\pm\sigma_{-+} \mp \sigma_{+-} + \sigma_{--} - \sigma_{++})}{(\sigma_{-+} + \sigma_{+-} + \sigma_{--} + \sigma_{++})(\pm\sigma_{-+} \mp \sigma_{+-} - \sigma_{--} + \sigma_{++})}}, \quad (15)$$

where  $\sigma_{+-}$  is the total cross section measured for right-handed positron beam and left-handed electron beam ( $\sigma_{--}$ ,  $\sigma_{+-}$  and  $\sigma_{-+}$  are defined analogously) and  $P_{e^+}$  ( $P_{e^-}$ ) is the resulting positron (electron) beam polarization.

### 5.1.2 Application

The total cross section is given by:

$$\sigma = \frac{N_{sig}}{\mathcal{L} \cdot \epsilon_{sig}}, \quad (16)$$

where  $N_{sig}$  is the number of selected signal events,  $\mathcal{L}$  is the luminosity and  $\epsilon_{sig}$  is the signal selection efficiency. The selection efficiency is defined, as usual, as the percentage of signal events satisfying the selection criteria.

The number of selected signal events,  $N_{sig}$ , is obtained from the number of selected events  $N_{tot}$ , rescaled in order to account for a residual background contamination. First, the purity  $P_{sig+\tau}$  is defined, which expresses the fraction of signal and tau-signal events in the total amount of selected events:

$$P_{sig+\tau} = \frac{N_{sig+\tau}}{N_{tot}}. \quad (17)$$

The number of signal and tau-signal events  $N_{sig+\tau}$  is, consequently, calculated as:

$$N_{sig+\tau} = N_{tot} \cdot P_{sig+\tau}. \quad (18)$$

Finally,  $N_{sig}$  is obtained from  $N_{sig+\tau}$ :

$$N_{sig} = \frac{N_{sig+\tau}}{1 + \frac{BR_\tau \cdot \epsilon_\tau}{BR_{sig} \cdot \epsilon_{sig}}}, \quad (19)$$

where  $BR_\tau$  ( $BR_{sig}$ ) is the known branching ratio of a  $W$ -boson decaying into a tau lepton and its associated neutrino (towards a muon or an electron and associated neutrino).

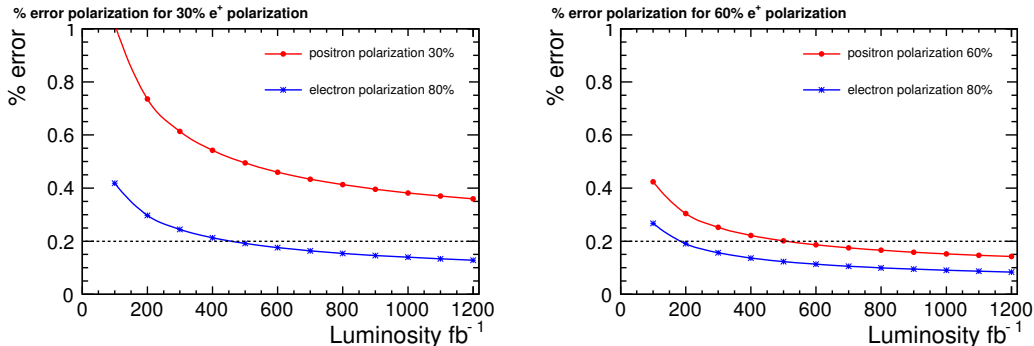


Figure 13: *Statistical precision on the polarization obtained with the modified Blondel scheme. Left: results for the low polarization case, with 80% electron beam and 30% positron beam polarization. Right: results for the 60% positron polarization option. The red (blue) curves show the percentage error on the positron (electron) polarization as a function of the total luminosity, which is assumed to be shared equally between the four polarization sets. The horizontal line indicates the optimum precision of 0.2%.*

The efficiency  $\epsilon_\tau$  is the percentage of tau-signal events satisfying the selection criteria. In the error propagation the experimental uncertainties on the branching ratios are assumed to be negligible with respect to those on the efficiencies.

The four cross sections  $\sigma_{+-}$ ,  $\sigma_{--}$ ,  $\sigma_{+}$  and  $\sigma_{-}$  have been measured using Monte Carlo samples for an integrated luminosity of  $20 \text{ fb}^{-1}$ . Equation 15 has then been applied and the statistical uncertainty on the measured polarizations has been calculated. The error has been propagated towards higher luminosities, as shown in Fig. 13 for both polarization options. The distribution on the left (right) shows the results obtained with 80% electron and 30% (60%) positron polarization. The total luminosity is assumed to be shared equally between the four polarization sets. For an integrated luminosity of  $500 \text{ fb}^{-1}$  and a high polarization of the positron beam the precision obtained on the electron and positron polarizations is  $\sim 0.1\%$  and  $\sim 0.22\%$ , respectively. In case of a 30%-polarized positron beam, precisions of the order of 0.5% on the positron polarization and 0.2% on the electron polarization are obtained, respectively. Considering the goal of a precision of the order of 0.2% on the polarization, the low positron polarization option appears strongly unfavoured.

## 5.2 The Angular Fit

The Blondel scheme requires high luminosities in order to obtain small uncertainties on the polarization. This motivates the quest of alternative techniques. In this section another method is described, denominated *angular fit*, which relies on the  $\cos\theta_W$  observable (defined in Sec. 4.2). In this way, also the additional information relative to the  $W$ -pair production angle is exploited in the polarization measurement, while the Blondel technique uses exclusively the total cross section information. The total cross section still enters the measurement via the normalization of the  $\cos\theta_W$  distributions.

The angular fit method is based on the creation of Monte Carlo templates of the  $\cos\theta_W$  distribution for several sets of the beam polarization. The  $\cos\theta_W$  distributions of the data

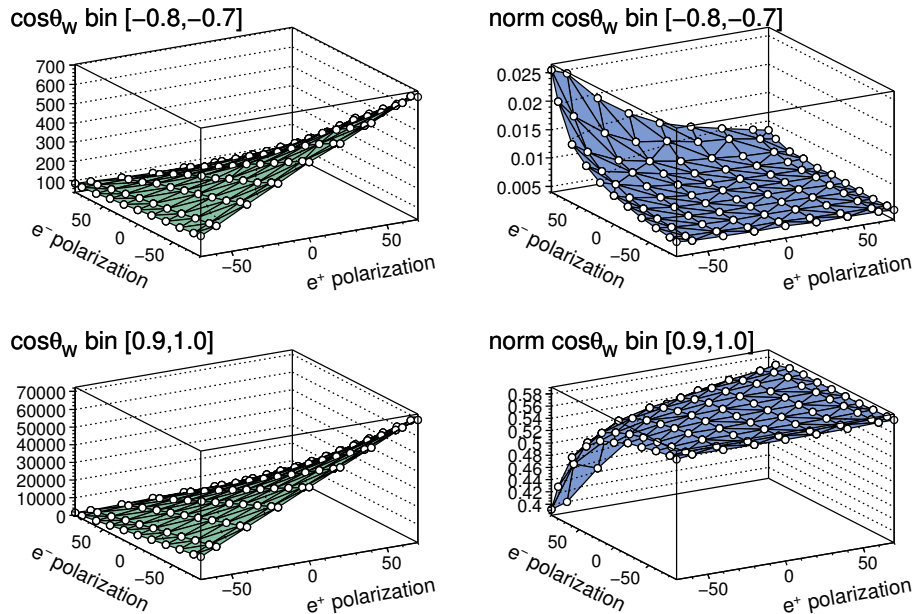


Figure 14: Content of the bins of the  $\cos\theta_W$  distribution as a function of the positron and electron beam polarization. The distributions on the right are created using normalized  $\cos\theta_W$  distributions. The upper (lower) distributions refer to the bin covering the  $\cos\theta_W$  range  $[-0.8, -0.7]$  ( $[0.9, 1.0]$ ), a region where the  $s$ -channel ( $t$ -channel) production prevails.

are fitted to the templates in order to measure the polarization. The creation of the templates and the structure of the fit are described in the following.

### 5.2.1 Templates of $\cos\theta_W$

The Monte Carlo files are mixed (Sec. 4.1) in order to create 99 samples with different polarizations, scanning the polarization of the electron (positron) in the interval  $[-90\%, +90\%]$  ( $[-70\%, +70\%]$ ). The selection (Sec. 4.2) is applied to each sample, obtaining 99  $\cos\theta_W$  distributions, one for each polarization set. Each distribution is divided into 20 bins, which cover the full range of variability of  $\cos\theta_W$   $[-0.95, +1]$ . For each bin the three-dimensional distribution of the bin content vs. the polarization of electron and positron is created. These distributions are filled with 99 points, corresponding to the 99 polarization sets considered. The results for two of the 20  $\cos\theta_W$  bins are illustrated in Fig. 14 (left). The distributions reflect clearly the total cross section dependency on the polarization of the beams (cf. Fig. 6). They have been created using Monte Carlo samples corresponding to an integrated luminosity of  $20 \text{ fb}^{-1}$  for each polarization set.

The same procedure has been repeated using normalized  $\cos\theta_W$  distributions. The normalization cancels the contribution from the total cross section, leaving only the information relative to the angle of production of the  $W$ -pair, which is the additional observable introduced with respect to the Blondel scheme. The results are shown in Fig. 14 (right).

Different topologies and a different dependency on the polarization are expected, depending on the production diagram of the  $W$ -pair (Sec. 3). This is confirmed by comparing the two diagrams generated from normalized  $\cos\theta_W$  distributions. The upper (lower) distribution in Fig. 14 (right) refers to the bin covering the  $\cos\theta_W$  range  $[-0.8, -0.7]$  ( $[0.9, 1.0]$ ), a region where the  $s$ -channel ( $t$ -channel) production prevails. The expected  $t$ -channel suppression for left-handed positrons and right-handed electrons is clearly visible in the lower distribution, while the upper distribution shows the clear relative enhancement of the  $s$ -channel contribution for this polarization combination.

For the purpose of measuring the polarization the distributions for non-normalized  $\cos\theta_W$  distributions are used, since they contain the additional information of the total cross section. In order to find a continuous function of the beam polarization, they are fitted with 2D quadratic functions. An illustrative example of a fitted surface is shown in Fig. 15 (left). The 20 2D-functions obtained for the 20  $\cos\theta_W$  bins are called *templates* in the following.

It should be noted that the background events surviving the selection have not been subtracted, when creating the distributions in Fig. 14, since the smoothness of the distribution is not spoiled by the presence of the residual background. This benefits the error propagation in the polarization measurement (details of the fit procedure are given in the following). The smoothness of the distributions is confirmed by the distribution on the right-hand side in Fig. 15, which shows the deviations of one of the template functions (namely for the  $\cos\theta_W$  bin  $[0.9, 1.0]$ ) from the discrete points it fits. The residuals are always below one sigma. Statistically, deviations up to three sigma would be expected. The fact that the deviations are so remarkably small is due to statistical independence reasons. The discrete points of the distributions come from the same Monte Carlo sample. For obvious CPU time convenience a new Monte Carlo sample was not simulated for each of the 99 polarization configurations considered. The same Monte Carlo files for 100% polarized beams have been mixed repeatedly to create the 99 different polarization sets. This does not introduce a bias, since there is no error associated to the Monte Carlo templates in the polarization extraction fit. The statistical error of the Monte Carlo templates can be easily reduced with respect to the error on the data in a real experiment, producing Monte Carlo samples for higher luminosities. What is relevant, is the statistical independence of the Monte Carlo sample taking the role of data. This is assured by random smearings, as explained in the following.

### 5.2.2 Performance of the Angular Fit

For a direct comparison with the modified Blondel scheme, the angular fit was first applied to the same data set and making the same assumption, that while reversing the sign of the polarization the absolute value remains the same. The data set consists again of four samples for the  $++$ ,  $+-$ ,  $-+$  and  $--$  helicity combinations. The total integrated luminosity is shared equally between the four samples. At the end of this section the performance of the fit is also investigated for different conditions.

The  $\cos\theta_W$  distributions for the data are obtained directly from the templates. The content of each bin of the distributions is derived from the template specific for that bin, evaluating the function for the desired polarization of the beams. In order to assure statistical independence a Poissonian random smearing is applied to the value obtained. As already mentioned, the original templates have been created for an integrated luminosity of  $20 \text{ fb}^{-1}$ , but the results are propagated to higher luminosities changing the normalization of the template functions. The data distributions are fitted to the templates using MINUIT [23]

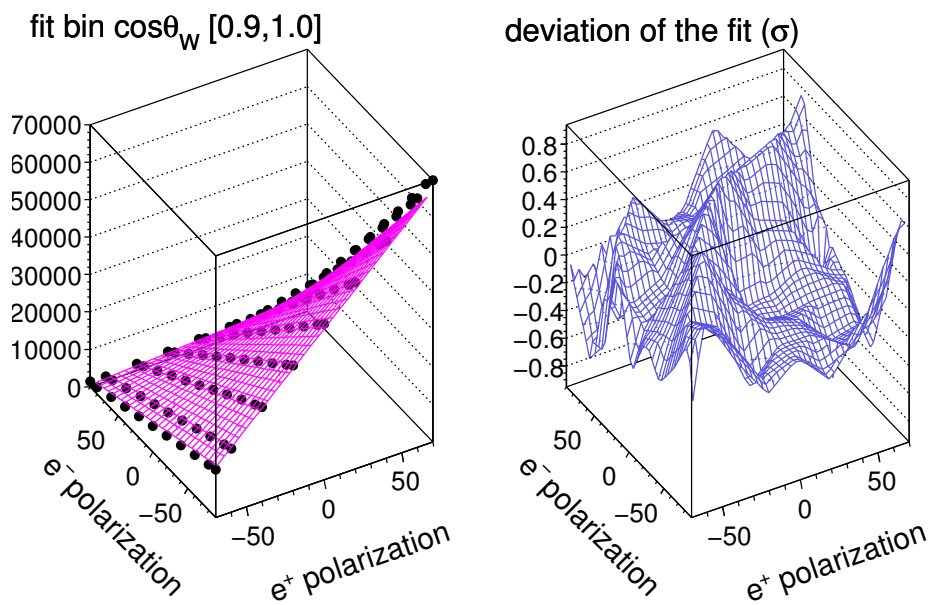


Figure 15: Left: content of the bin of the  $\cos\theta_W$  distribution, covering the range  $[0.9,1.0]$ , as a function of the polarization of the positron and electron beam. The two-dimensional function fitting the distribution is also drawn. Right: deviations of the fitting surface from the discrete points, expressed in number of sigmas.

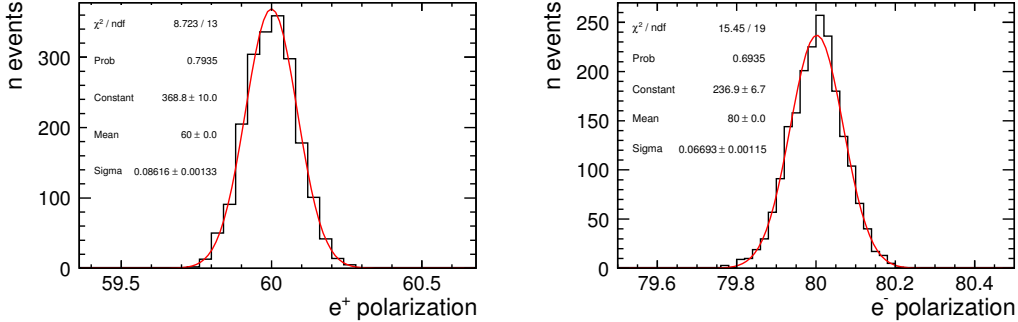


Figure 16: Distributions of the fitted parameters when applying the angular fit with two free parameters, the absolute values of the electron and the positron beam polarizations. The left (right) distribution shows the distribution of the fitted positron (electron) polarization for the option of 60% positron and 80% electron polarization and for an integrated luminosity of  $500 \text{ fb}^{-1}$ . The fit statistical errors on the measured polarizations are given by the widths of the fitted Gaussians.

and a  $\chi^2$  minimization. The  $\chi^2$  function is defined as:

$$\chi^2 = \sum_{j=1}^4 \sum_{i=1}^{20} \frac{(N_{i,j}^{DATA} - f_i(\pm P_{e^+}, \pm P_{e^-}))^2}{N_{i,j}^{DATA}}, \quad (20)$$

where  $N_{i,j}^{DATA}$  is the content of the  $i$ -th bin of the  $\cos \theta_W$  distribution for the  $j$ -th data sample of the four data samples for the different helicity sets. The Monte Carlo template  $f_i$  for the same bin of  $\cos \theta_W$  and the polarizations  $P_{e^+}$  and  $P_{e^-}$  depend on the sample  $j$ .

The fit has first been performed with two free parameters, the absolute value of the polarizations of the beams. For each considered luminosity the fit is repeated several times, changing randomly the Poissonian smearing of the data distributions for each iteration. The resulting fitted parameters are Gaussian distributed around the expected value, as shown in Fig. 16. The fit statistical errors are obtained from the widths of the Gaussian fitted to the parameter distributions.

The error determination has been checked like this in order not to trust blindly the MINUIT output. Moreover, with this technique it is possible to check not only the correct distributions of the fitted parameters, but also the behavior of the fit probability and the correlations between the parameters.

The fit probability is shown in Fig. 17 (e.g. for 60% positron and 80% electron polarization and for an integrated luminosity of  $500 \text{ fb}^{-1}$ ). It is flat as expected for a correct fit. The correlation between the two fit parameters is negligible for both positron polarization options (see Tab. 4).

The precision achieved with the angular fit method is summarized in Fig. 18, where it is compared with the Blondel method. For the 60% positron polarization option and a total luminosity of  $250 \text{ fb}^{-1}$  (Fig. 18, right) the desired relative precision of 0.2% is obtained for both polarizations. In case of low positron polarization an integrated luminosity of  $1200 \text{ fb}^{-1}$  is needed to achieve the same uncertainty. In this case, with an integrated luminosity of

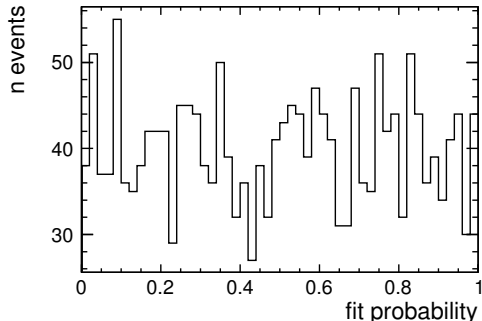


Figure 17: *Distribution of the fit probability for the angular fit with two free parameters for the option of 60% positron and 80% electron polarization and an integrated luminosity of  $500 \text{ fb}^{-1}$ .*

| $e^+$ pol | % ++ -- | $\Delta P_{e^+}/P_{e^+}\%$ | $\Delta P_{e^-}/P_{e^-}\%$ | corr% |
|-----------|---------|----------------------------|----------------------------|-------|
| 30        | 50      | 0.34                       | 0.08                       | 6.6   |
| 60        | 50      | 0.14                       | 0.08                       | 3.4   |
| 60        | 20      | 0.18                       | 0.11                       | 33.4  |
| 60        | 10      | 0.23                       | 0.14                       | 58.4  |

Table 4: *Summary of the results obtained with the angular fit method for a total integrated luminosity of  $500 \text{ fb}^{-1}$ . The percentage of the total luminosity spent on the same-sign helicity configurations of the beams is shown in the second column. The results are shown for an electron polarization of 80%, while both positron polarization options are considered:  $P_{e^+} = 30\%$  and  $P_{e^+} = 60\%$ .*

$500 \text{ fb}^{-1}$  precisions of  $\sim 0.1\%$  on the electron polarization and of  $\sim 0.35\%$  on the positron polarization are obtained.

The angular fit appears to be more powerful than the modified Blondel scheme, yielding the same precisions at much lower luminosities.

For the 60% positron polarization option the performance of the fit has also been studied reducing the luminosity spent on the ++ and -- polarization sets. Such configurations of the helicities are of low interest for most of the physics studies, since they suppress the  $s$ -channel production. The results obtained are shown in Fig. 19. When spending only 20% (10%) of the total luminosity on the same-sign polarization sets, precisions of  $\sim 0.1\%$  on the electron polarization and of  $\sim 0.2\%$  on the positron polarization are obtained at  $400 \text{ fb}^{-1}$  ( $600 \text{ fb}^{-1}$ ). In case the luminosity is equally-shared between the four data samples, the same results are obtained at  $250 \text{ fb}^{-1}$ .

The correlation between the fitted polarizations increases when reducing the amount of luminosity spent on the same-sign helicity sets. However, even reducing the percentage of luminosity spent on the same-sign configurations to only 10%, the correlation between the fitted parameters is still acceptable.

The results obtained with the angular fit method for an integrated luminosity of  $500 \text{ fb}^{-1}$  are summarized in Tab. 4.

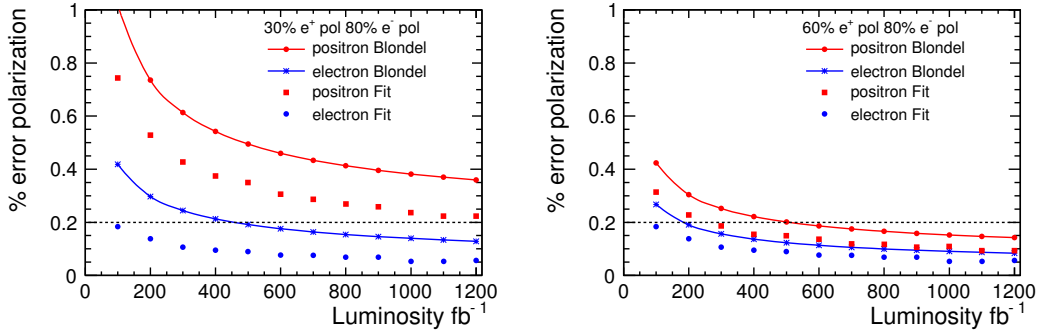


Figure 18: Comparison of the results obtained with the modified Blondel scheme (continuous curves) and with the angular fit method (dots). The distribution on the left (right) shows the results obtained for the low (high) polarization option, with 80% electron and 30% (60%) positron polarization. The red (blue) curves show the percentage error on the positron (electron) polarization as a function of the total luminosity, which is shared equally between the four polarization sets.

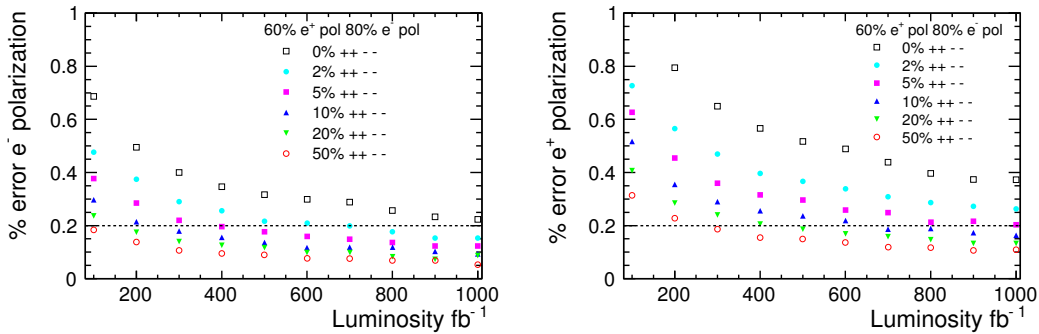


Figure 19: Results obtained with the angular fit method, in the 60% polarization option. The distribution on the left (right) shows the percentage error on the electron (positron) beam polarization as a function of the total luminosity. The different curves are obtained spending different percentages of the total luminosity with the same helicity for both beams, according to the legend.

|                         | $R_1$  | $R_2$  | $R_3$  | $R_4$  | $R_5$  | $R_6$  | $R_7$  | $R_8$  | $R_9$  |
|-------------------------|--------|--------|--------|--------|--------|--------|--------|--------|--------|
| $\Delta g_1^Z$          | +0.001 | 0      | 0      | -0.001 | 0      | 0      | +0.001 | 0      | +0.001 |
| $\Delta \kappa_\gamma$  | 0      | +0.001 | 0      | 0      | -0.001 | 0      | +0.001 | +0.001 | 0      |
| $\Delta \lambda_\gamma$ | 0      | 0      | +0.001 | 0      | 0      | -0.001 | 0      | +0.001 | +0.001 |

Table 5:  $\Delta g_1^Z$ ,  $\Delta \kappa_\gamma$  and  $\Delta \lambda_\gamma$  values used to calculate the coefficients in Eq. 21.

## 6 Triple Gauge Couplings and Polarization

In this section the simulation of the TGCs using Whizard is illustrated and the additional angular observables introduced to gain sensitivity to the TGCs are described. The systematic impact that anomalous values of the TGCs might have on the performance of the partial measurement of the only polarization is calculated. Finally, an extension of the angular fit method is discussed, which allows a simultaneous measurement of the TGCs in addition to the beam polarizations.

Only three independent couplings are considered,  $g_1^Z$ ,  $\kappa_\gamma$  and  $\lambda_\gamma$ , as in the LEP analysis (Sec. 2). Thanks to the foreseen high luminosity of the ILC, these couplings can be measured simultaneously, while in the LEP analysis they are measured in single fits, where one parameter is allowed to vary and the other two are fixed.

### 6.1 Simulation of the Triple Gauge Couplings

In order to perform a fit, it is necessary to associate a weight to the Monte Carlo events. This weight is expressed as a continuous function of the TGCs:

$$\begin{aligned}
R(\Delta g_1^Z, \Delta \kappa_\gamma, \Delta \lambda_\gamma) = & 1 + A\Delta g_1^Z + B\Delta \kappa_\gamma + C\Delta \lambda_\gamma + D\Delta g_1^{Z^2} + E\Delta \kappa_\gamma^2 + F\Delta \lambda_\gamma^2 \\
& + G\Delta g_1^Z \Delta \kappa_\gamma + H\Delta g_1^Z \Delta \lambda_\gamma + I\Delta \lambda_\gamma \Delta \kappa_\gamma,
\end{aligned} \tag{21}$$

where the function  $R(\Delta g_1^Z, \Delta \kappa_\gamma, \Delta \lambda_\gamma)$  describes the quadratic dependence of the differential cross sections on the three TGCs [2], and the  $\Delta$  in front of the TGC names indicates that they are expressed as deviations from the SM value. The nine coefficients in Eq. 21 are obtained calculating the value assumed by  $R(\Delta g_1^Z, \Delta \kappa_\gamma, \Delta \lambda_\gamma)$  for the nine sets of TGCs shown in Tab. 5.

The calculation of the weight for these specific values of the couplings is performed using the same WHIZARD configuration used in the event generation. WHIZARD allows to rescan a given event sample, recalculating the matrix element values event-by-event with some modification applied. As a result, each event is assigned a weight, which takes into account the changes due to the different TGC values without modifying the event kinematics. This procedure is perfectly suitable for small tunings of some parameters, such as requiring an anomalous value of the TGCs. With this technique nine weights  $R_i$ ,  $i = 1, 2, \dots, 9$  are obtained, for the nine sets of TGCs in Tab. 5:

| Parameter        | 68% C.L.                   | Nominal Value |
|------------------|----------------------------|---------------|
| $g_Z^1$          | $0.984^{+0.022}_{-0.019}$  | 1             |
| $\kappa_\gamma$  | $0.973^{+0.044}_{-0.045}$  | 1             |
| $\lambda_\gamma$ | $-0.028^{+0.020}_{-0.021}$ | 0             |

Table 6: The 68% C.L. values for the three TGCs obtained from a combination of ALEPH, L3 and OPAL results. In each case the parameter listed is varied while the other two are fixed to their SM values. Both statistical and systematic errors are included. From [8].

$$\begin{aligned}
R_1 &= 1 + A |\Delta g_1^Z| + D |\Delta g_1^Z|^2, \\
R_2 &= 1 + B |\Delta \kappa_\gamma| + E |\Delta \kappa_\gamma|^2, \\
R_3 &= 1 + C |\Delta \lambda_\gamma| + F |\Delta \lambda_\gamma|^2, \\
R_4 &= 1 - A |\Delta g_1^Z| + D |\Delta g_1^Z|^2, \\
R_5 &= 1 - B |\Delta \kappa_\gamma| + E |\Delta \kappa_\gamma|^2, \\
R_6 &= 1 - C |\Delta \lambda_\gamma| + F |\Delta \lambda_\gamma|^2, \\
R_7 &= 1 + A |\Delta g_1^Z| + B |\Delta \kappa_\gamma| + D |\Delta g_1^Z|^2 + E |\Delta \kappa_\gamma|^2 + G |\Delta g_1^Z| |\Delta \kappa_\gamma|, \\
R_8 &= 1 + B |\Delta \kappa_\gamma| + C |\Delta \lambda_\gamma| + E |\Delta \kappa_\gamma|^2 + F |\Delta \lambda_\gamma|^2 + I |\Delta \kappa_\gamma| |\Delta \lambda_\gamma|, \\
R_9 &= 1 + A |\Delta g_1^Z| + C |\Delta \lambda_\gamma| + D |\Delta g_1^Z|^2 + F |\Delta \lambda_\gamma|^2 + H |\Delta g_1^Z| |\Delta \lambda_\gamma|, \quad (22)
\end{aligned}$$

where  $|\Delta g_1^Z| = |\Delta \kappa_\gamma| = |\Delta \lambda_\gamma| = 0.001$ . The value 0.001 is chosen, since it is the approximate order of magnitude of the expected precision. Inverting these equations one derives the nine coefficients  $A, B, C, D, E, F, G, H, I$  to be inserted into Eq. 21. The procedure is repeated for each signal and tau-signal event, obtaining an individual expression of  $R(\Delta g_1^Z, \Delta \kappa_\gamma, \Delta \lambda_\gamma)$  for each event. The impact of the TGCs on the small residual background contamination of the event samples has been neglected.

## 6.2 Triple Gauge Couplings Impact

As motivated above, a precise measurement of the TGCs is extremely important in itself. However, in this section it is shown that anomalous values of the TGCs might affect the measurement of the polarization from the  $W$ -pair channel in a non-negligible way, further motivating the study of a simultaneous fit.

Tab. 6 summarizes the final 68% C.L. TGCs values obtained at LEP combining the results from ALEPH, L3 and OPAL, already discussed in Sec. 2.

The limits set by the LEP experiments are weak relative to the excellent performance required for the polarization measurement at the ILC and might have a non-negligible systematic impact. This can easily be seen by changing the values of the TGCs in the Monte Carlo “data” sample and repeating the polarization measurement. Using the reweighting technique one coupling at a time was varied from its SM tree-level value used for the standard event generation to either the upper, or the lower  $1\text{-}\sigma$  limit set by the LEP experiments. For example  $g_Z^1$  has been changed from 1 to  $1.202 (= 0.984 + 0.022)$  and to  $0.965 (= 0.984 - 0.019)$ . The Blondel scheme and the angular fit method have been applied, using the Monte Carlo

| 60% positron polarization |                       |         |        |                 |        |                  |        |
|---------------------------|-----------------------|---------|--------|-----------------|--------|------------------|--------|
|                           | coupling              | $g_Z^1$ |        | $\kappa_\gamma$ |        | $\lambda_\gamma$ |        |
|                           | $\Delta$              | 0.006   | -0.035 | 0.017           | -0.072 | -0.008           | -0.049 |
| Fit                       | $\Delta pol_{e^+} \%$ | -0.12   | 0.46   | 0.15            | -1.18  | -0.01            | 0.25   |
|                           | $\Delta pol_{e^-} \%$ | -0.15   | 0.55   | 0.24            | -1.59  | 0.00             | 0.23   |
| Blondel                   | $\Delta pol_{e^+} \%$ | -0.04   | 0.17   | 0.02            | -0.39  | -0.01            | 0.24   |
|                           | $\Delta pol_{e^-} \%$ | -0.04   | 0.18   | 0.04            | -0.61  | 0.00             | 0.16   |
| 30% positron polarization |                       |         |        |                 |        |                  |        |
|                           | coupling              | $g_Z^1$ |        | $\kappa_\gamma$ |        | $\lambda_\gamma$ |        |
|                           | $\Delta$              | 0.006   | -0.035 | 0.017           | -0.072 | -0.008           | -0.049 |
| Fit                       | $\Delta pol_{e^+} \%$ | -0.15   | 0.60   | 0.17            | -1.34  | -0.03            | 0.14   |
|                           | $\Delta pol_{e^-} \%$ | -0.20   | 0.69   | 0.33            | -2.17  | 0.00             | 0.26   |
| Blondel                   | $\Delta pol_{e^+} \%$ | -0.04   | 0.23   | 0.01            | -0.25  | -0.03            | -0.14  |
|                           | $\Delta pol_{e^-} \%$ | -0.04   | 0.18   | 0.05            | -0.61  | 0.00             | 0.14   |

Table 7: Systematic uncertainty on the polarization measurement introduced by anomalous values of the TGCs. The upper (lower) part of the table refers to the 60% (30%) positron polarization option. The TGCs are changed, one at a time, by a difference  $\Delta$  from the SM tree-level value, leaving the others fixed. The chosen differences  $\Delta$  are the maximum deviations from the SM, allowed by the LEP 68% C.L. limits. The deviations of the measured positron (electron) polarizations  $\Delta pol_{e^+}$  ( $\Delta pol_{e^-}$ ) from the true values are also indicated.

samples with anomalous values of the TGCs as “data”. The results obtained are summarized in Tab. 7.

The systematic uncertainty introduced by propagating the experimental error on the TGCs is too high, when considering that precisions of the order of 0.2% on the polarizations are desired. The angular fit method would allow to control the effect of the TGCs by monitoring the  $\chi^2$  (which would be blown up by wrong assumptions on the values of the couplings). The full capabilities of the angular fit method can be exploited by implementing a simultaneous fit of the TGCs and the polarization. In order to gain sensitivity to the couplings new observables are introduced into the fit. They are described in the following.

### 6.3 Decay Angles of the W-pair

In order to maximize the sensitivity to the TGCs, two more observables are introduced characterizing the leptonic decay of the  $W$ -boson. A  $W$ -pair event is described by five angles, as illustrated in Fig. 20.

The angle  $\theta_W$ , already introduced previously, is the angle between the incoming electron beam and the outgoing  $W^-$ . The four angles  $\cos\theta^*$  and  $\phi^*$  describe the decays of the two  $W$ -bosons in their rest frame. They are defined as the angles of the down-type decay product  $f_d$  in the right-handed coordinate system of the  $W$ -boson rest frame, where the two decay products are back-to-back. The  $z$ -axis of each decay coordinate system coincide with the parent  $W$ -boson direction in the overall center-of-mass system, while the  $y$ -axes direction is given by  $\vec{e}^- \times \vec{W}$ , where  $\vec{e}^-$  is the direction of the incoming electron beam and  $\vec{W}$  is the flight direction of the parent  $W$ -boson. The decay angles can be classified corresponding to the decay type (hadronic or leptonic). The angles describing the hadronic (leptonic) decay

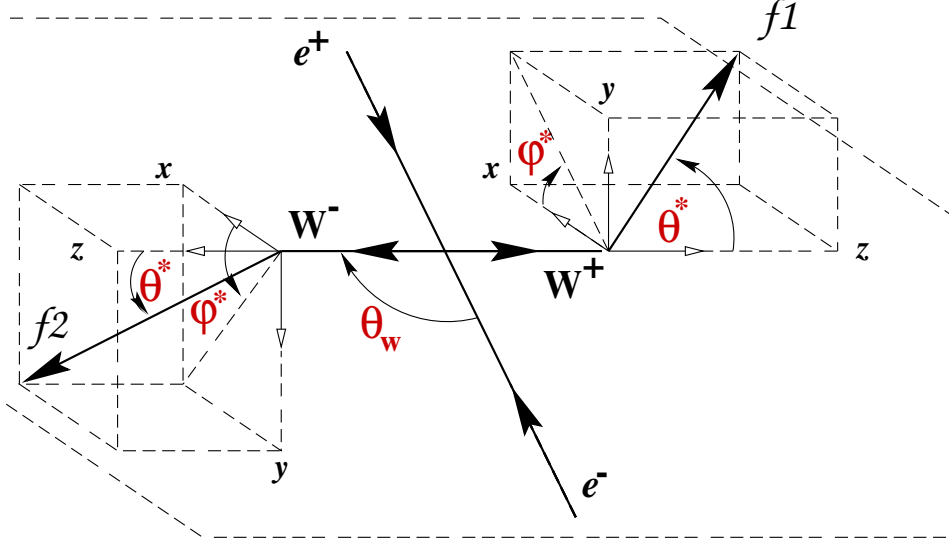


Figure 20: Definition of the angles in an  $e^+e^- \rightarrow W^+W^-$  event.

are called  $\cos\theta_h^*$  ( $\cos\theta_l^*$ ) and  $\phi_h^*$  ( $\phi_l^*$ ).

The hadronic decay angles suffer from a two-fold ambiguity, due to the unknown charge of the quarks. The two quarks are back-to-back in the rest frame of the  $W$ -boson and the resulting ambiguity is:

$$(\cos\theta_h^*, \phi_h^*) \leftrightarrow (-\cos\theta_h^*, \phi_h^* + \pi), \quad (23)$$

which is folded in the following way:

$$\begin{aligned} \phi_h^* > 0 &\rightarrow (\cos\theta_h^*, \phi_h^*) \\ \phi_h^* < 0 &\rightarrow (-\cos\theta_h^*, \phi_h^* + \pi). \end{aligned} \quad (24)$$

However, for the present study only the angles describing the leptonic decay are used. Their distributions are shown in Fig. 21, with the respective resolutions. Fig. 22 compares the  $\cos\theta_W$  distribution with no anomalous TGCs with a scenario in which an anomalous value was assigned to the  $g_1^Z$  coupling in order to exemplify the impact of the TGCs on the angular observables.

#### 6.4 Simultaneous Fit

The distributions used in the combined fit are multi-dimensional distributions of the angular observables. With all four decay angles, in addition to the  $\cos\theta_W$  observable, one would need five-dimensional distributions. Filling a five-dimensional distribution leads to poor statistics for the single bins and does not appear to be a convenient choice. It was therefore decided to move to three-dimensional distributions, using only the angles which describe the leptonic decay  $\cos\theta_l^*$  and  $\phi_l^*$ , together with  $\cos\theta_W$ . This choice is also supported by the fact

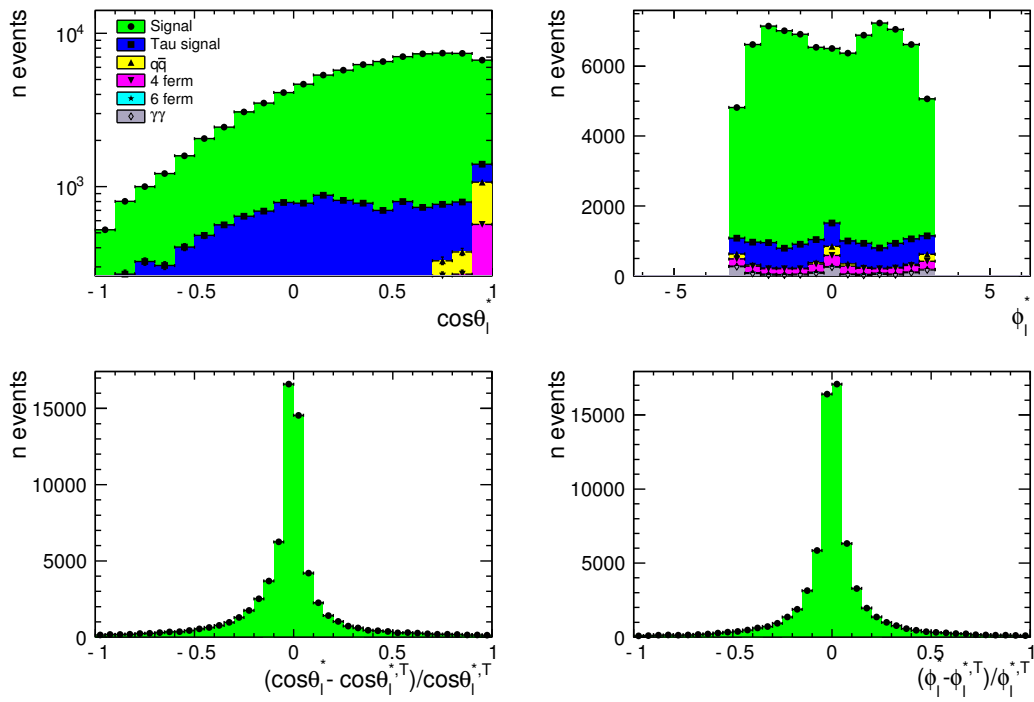


Figure 21: Decay angles (top panels) and their respective resolutions (bottom panels) for the leptonically decaying  $W$ -boson. Left: polar angle  $\cos\theta_l^*$ . Right: azimuthal angle  $\phi_l^*$ . The true Monte Carlo decay angles are denoted  $\cos\theta_l^{*,T}$  and  $\phi_l^{*,T}$ , respectively.

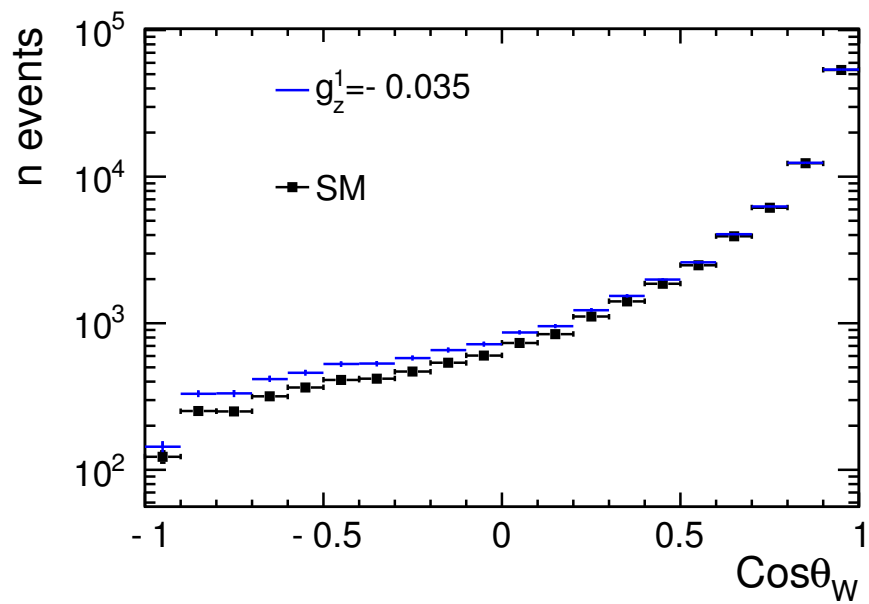


Figure 22: Comparison of two  $\cos \theta_W$  distributions: the black squares show the SM distribution, while the blue markers show the distribution obtained for a simulated anomalous value of the  $g_1^Z$  coupling, namely  $g_1^Z = -0.035$ .

that these angles are not affected by the two-fold ambiguity, while the remaining, unused angles  $\cos\theta_h^*$  and  $\phi_h^*$  are.

A Monte Carlo template of the three-dimensional distribution has been created for  $30\text{ fb}^{-1}$  of luminosity. As for the angular fit of the polarization only, the results have then been propagated to higher luminosities, rescaling the original distributions accordingly.

The “data” are created from the Monte Carlo template, reweighting the events for anomalous values of the TGCs and the desired polarizations. The fit shows slightly different performances for different values of the couplings. Slightly better performances are obtained for values of the couplings far from the SM tree-level expectations. Therefore, the fit was optimized for TGCs coincident with the SM tree-level values, since this option gives the most conservative estimate of the fit uncertainties.

A Poissonian random variation of the content of the 3D-bins of the data distributions is applied, in order to assure statistical independence from the Monte Carlo template sample.

When fitting the template distributions to the data, two weights are applied to each event of the template. One weight is a function of the TGCs (cf. Eq. 21) and one of the polarization (Sec. 4.1). Since the correlation between the TGCs and the polarization of the incoming beams is negligible, the weights factorize as follows:

$$weight = R(\Delta g_1^Z, \Delta\kappa_\gamma, \Delta\lambda_\gamma) * weight(P_{e^+}, P_{e^-}), \quad (25)$$

where the function  $R$  was already introduced in Eq. 21 and  $P_{e^\pm}$  are the beam polarizations. No  $R$  weight has been associated to the background events. The weight that expresses the dependence on the polarization was already discussed in Sec. 4.1.

The choice of the binning of the three-dimensional distributions is crucial. The polarization is mainly sensitive to the total cross section information, i.e. to the normalization of the distributions, as clearly shown in Fig. 14. A finer binning leads to a higher sensitivity to the shape of the distributions and in general increases the sensitivity to the TGCs, though decreasing the statistics in each bin.

The procedure applied in order to estimate the error of the fit takes into account both the precision and the statistical issues. The fit is repeated several times, each time using a different “data” sample. The different “data” samples were obtained from the same simulated distribution but with a different Poissonian variation, similar to what was done for the angular fit of the polarization only. A too fine binning, leading to poor statistics in most of the bins of the 3D angular distributions, causes the fit to not converge at all or to give non-Gaussian or off-centered distributions of the parameters. An example of a fit suffering from a statistical issue, due to the choice of a too fine binning for the considered luminosity, is shown in Fig. 23 (left). The distribution of the measured positron polarization is clearly off-center with respect to the expected value (60) and it is non-Gaussian. The right distribution in the same Figure shows the outcome of a correct fit: the distribution of the fitted parameter is Gaussian and centered around the expected value.

The fit has been repeated both as a log-likelihood minimization and as a  $\chi^2$  minimization. The first option is more stable in the low-statistics case, allowing a finer binning. The second technique has been used in order to check the goodness of the fit implementation, via the resulting  $\chi^2$  distribution, which has to be consistent with the degrees of freedom of the fit. This is possible since the performance of the fit at sufficiently high luminosities, where the  $\chi^2$  minimization is not dramatically affected by statistical issues, is similar for  $\chi^2$  and log-likelihood.

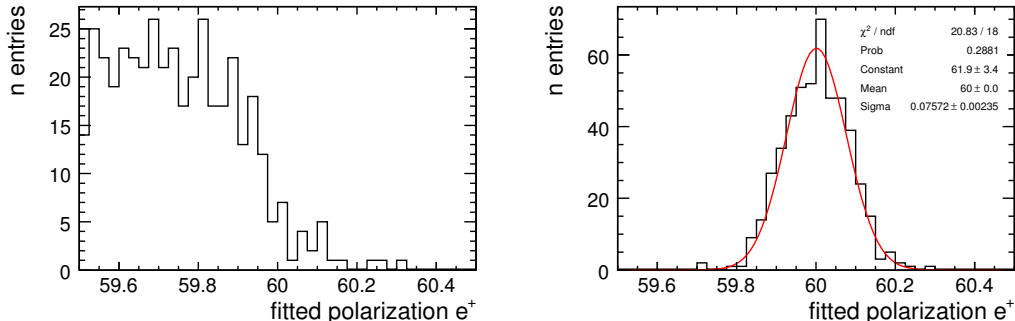


Figure 23: The left distribution shows an example of a fit suffering from too low statistics due to the choice of a too fine binning for the considered luminosity. The distribution of the measured positron polarization is clearly off-center with respect to the expected value (60) and non-Gaussian. On the right the same distribution is shown for a proper choice of the binning.

The  $\chi^2$  function is defined as:

$$\chi^2 = \sum_{++,--,+-,-+} \sum_{bins} \frac{(N_i^{MC}(P_{e^+}, P_{e^-}, TGCs) - N_i^{DATA})^2}{N_i^{DATA}}, \quad (26)$$

where  $N_i^{MC}(P_{e^+}, P_{e^-}, TGCs)$  is the content of the  $i$ -th bin of the Monte Carlo template, weighted as a function of polarization and TGCs, and  $N_i^{DATA}$  is the content of the corresponding bin for the “data” distribution. The sum  $\sum_{++,--,+-,-+}$  accounts for the fact that four different “data” samples are used, corresponding to the different helicity sets, as for the previous measurements.

The log-likelihood function is analogously defined as:

$$L = \sum_{++,--,+-,-+} \sum_{bins} (N_i^{DATA} \log N_i^{MC}(P_{e^+}, P_{e^-}, TGCs) - N_i^{MC}(P_{e^+}, P_{e^-}, TGCs)). \quad (27)$$

Where not otherwise specified, the results reported in the following are always meant as results of the log-likelihood fit.

The optimum binning chosen is: 10 bins for the  $\cos \theta_W$  distribution and 5 bins for each decay angle distribution. At high luminosities it is possible to move to a finer binning. Starting at a high luminosity of about  $500 \text{ fb}^{-1}$ , the log-likelihood fit is stable also using a binning of 20, 10, 10 for the  $\cos \theta_W$ ,  $\cos \theta_i^*$  and  $\phi_i^*$  distributions, respectively. The finer binning does not affect significantly the polarization measurement, as already explained, and no improvement can be observed for the measurement of  $g_1^Z$  and  $\kappa_\gamma$ . The sensitivity to  $\lambda_\gamma$  is the only one affected and is improved by a factor two. In Tab. 8 the results of the fit for the two different binnings are compared for a total luminosity of  $500 \text{ fb}^{-1}$ .

Cross-checks on the fit method have been performed using the  $\chi^2$  minimization and a Gaussian smearing of the data instead of the Poissonian one. In fact, the  $\chi^2$  is expected to follow a regular behavior only with Gaussian errors. The difference is generally negligible,

but due to the presence of low-statistics bins it is appropriate to use the Gaussian smearing to check the regular behavior of the minimization. The  $\chi^2$  and the fit probability distributions obtained are shown in the upper panels of Fig. 24 for a total luminosity of  $500 \text{ fb}^{-1}$  and a 10-5-5 binning. The  $\chi^2$  distribution should follow the behavior expected for 995 degrees of freedom. It was obtained, in fact, using  $10 \cdot 5 \cdot 5 = 250$  bins for each of the four data sets, which give 1000 bins in total. Since there are 5 free parameters in the fit, the absolute values of the two beam polarizations and the three couplings, the degrees of freedom are 995.

It is not possible to fit the  $\chi^2$  distribution with an analytical expression of the  $\chi^2$  function directly. In fact, the  $\Gamma$  functions entering the analytical expression diverge for such a high number of degrees of freedom. In any case the  $\chi^2$  function can be well approximated with a two-parameter Gaussian, constraining the width of the Gaussian to the square root of its mean value. Such a fit gives 1021 measured degrees of freedom, a value slightly higher than the expected one. This is mirrored by the fit probability distribution, which peaks at zero, while it is expected to be homogeneously distributed over the whole range  $[0,1]$ . The reason for such a behavior is due to the limited statistics used to produce the Monte Carlo sample ( $30 \text{ fb}^{-1}$ ). Though the number of events is scaled, when propagating the results to higher luminosities, there is still an uncertainty introduced by the low-statistics bins. These bins are affected by fluctuations, when the Monte Carlo 3D template distribution is filled with  $30 \text{ fb}^{-1}$  of events. These fluctuations are directly propagated to higher luminosities, since higher luminosities are obtained reweighting the events and not increasing the number of events. This effect would be canceled by producing a Monte Carlo sample for higher luminosities. A detailed explanation about this topic can be found in [24]. Since a larger Monte Carlo sample was not available, alternatively it was possible to balance the  $\chi^2$  by adding an error also for the Monte Carlo in the  $\chi^2$  function. Since the error is related to the initial number of events, not to the rescaled number of events, the error on the Monte Carlo enters the  $\chi^2$  definition as a simple rescaling. Eq. 26 becomes:

$$\chi^2 = \sum_{++,--,+-,-+} \sum_{bins} \frac{(N_i^{MC}(P_{e^+}, P_{e^-}, TGCs) - N_i^{DATA})^2}{N_i^{DATA} \cdot 1.025}, \quad (28)$$

where the value used to rescale the error in the denominator, 1.025, has been obtained empirically. The  $\chi^2$  and the fit probability distributions obtained after this change, are shown in the lower panels of Fig. 24. The fit of the  $\chi^2$  distribution returns the expected number of degrees of freedom and the fit probability distribution is flat. The resulting distributions of the fit parameters are not affected by the  $\chi^2$  redefinition. For consistency, the likelihood function was rescaled by the same factor, though the impact on the error of the measured fit parameters for such a tiny factor is negligible.

## 6.5 Results

In Fig. 25 the precision on the polarization achieved using the simultaneous fit for the TGCs is compared to the results obtained with the angular fit method of the polarization alone. The total luminosity is shared equally between the four polarization sets  $++$ ,  $+-$ ,  $-+$  and  $--$ . The graphs clearly show that there is no loss in the sensitivity to the polarization, when also fitting simultaneously the TGCs.

Fig. 26 shows the precision obtained for the TGCs. The precision is expressed as an absolute uncertainty. The results shown on the left (right) have been obtained with a binning of respectively 10 (20), 5 (10) and 5 (10) bins for the  $\cos\theta_W$ ,  $\cos\theta_i^*$  and  $\phi_i^*$  distributions.

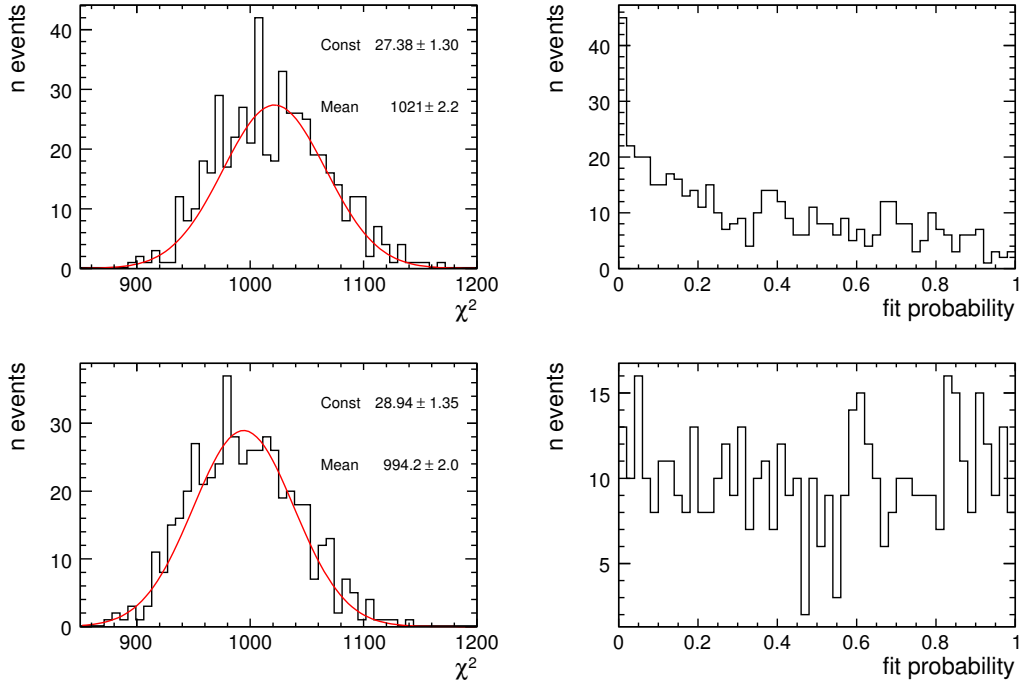


Figure 24: The upper panels show the  $\chi^2$  distribution (left) and the fit probability (right) distributions, obtained for an integrated luminosity of  $500 \text{ fb}^{-1}$  with a simultaneous  $\chi^2$  fit of TGCs and polarization. In the lower panels the same distributions are reproduced increasing the error which enters the  $\chi^2$  definition in order to account for the limited Monte Carlo statistics (Eq. 28).

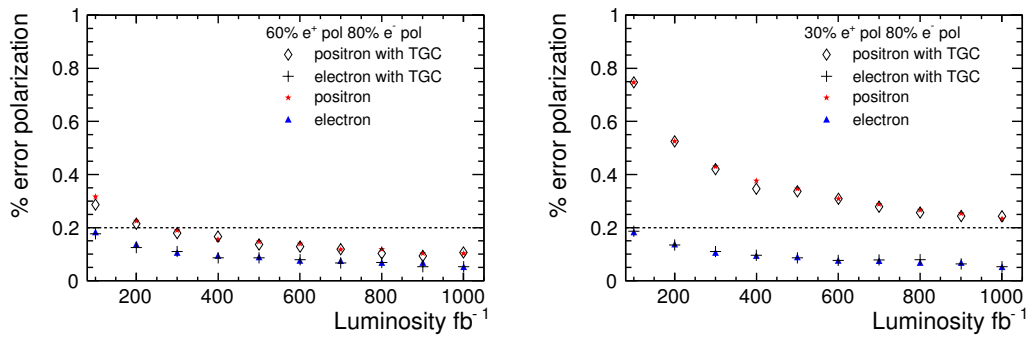


Figure 25: The precision on the polarization achieved by the simultaneous fit with the TGCs is compared to the results obtained with the angular fit method of the polarization alone. The graph on the left (right) refers to a positron polarization of 60% (30%).

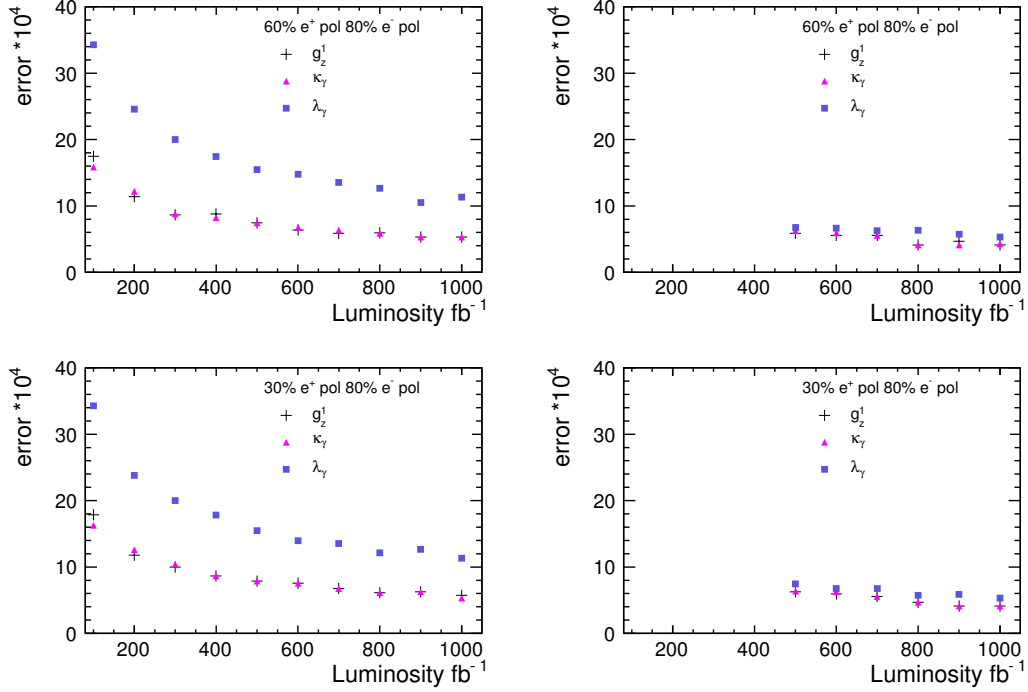


Figure 26: Absolute uncertainty on the TGCs obtained with the simultaneous fit of the TGCs the polarization of the beam. The upper (lower) distributions refer to a positron polarization of 60% (30%). The results shown on the left (right) have been obtained with a binning of respectively 10 (20), 5 (10) and 5 (10) bins for the  $\cos\theta_W$ ,  $\cos\theta_l^*$  and  $\phi_l^*$  distributions. The fit performed with the finest binning is stable only at high luminosities of more than  $500\text{ fb}^{-1}$ .

The fit performed with the finest binning is stable only at high luminosities of more than  $500\text{ fb}^{-1}$ .

The results for an integrated luminosity of  $500\text{ fb}^{-1}$  are summarized in Tab. 8, comparing the two different binnings, while the correlations between the measured fit parameters are reported in Tab. 9. The correlation between the electron and the positron polarizations and between the polarizations and the TGCs are small. The correlations between the couplings are higher, but acceptable. As already anticipated, only the uncertainty on the coupling  $\lambda_\gamma$  is affected in a non-negligible way by the binning, improving by about a factor 2 when the finest binning is employed.

The precision achievable for an integrated luminosity of  $500\text{ fb}^{-1}$  on the couplings is better than  $10^{-3}$  and could improve the current limits on the couplings by one order of magnitude.

| Parameter                              | bin 20-10-10 | bin 10-5-5 |
|--|--------------|------------|
| 60% $P_{e^+}$                          |              |            |
| $\Delta P_{e^+} \%$                    | 0.13         | 0.14       |
| $\Delta P_{e^-} \%$                    | 0.08         | 0.09       |
| $\Delta g_1^Z \cdot 10^{-04}$          | 5.9          | 7.3        |
| $\Delta \kappa_\gamma \cdot 10^{-04}$  | 6.2          | 7.4        |
| $\Delta \lambda_\gamma \cdot 10^{-04}$ | 6.9          | 15.3       |
| 30% $P_{e^+}$                          |              |            |
| $\Delta P_{e^+} \%$                    | 0.33         | 0.34       |
| $\Delta P_{e^-} \%$                    | 0.08         | 0.08       |
| $\Delta g_1^Z \cdot 10^{-04}$          | 6.1          | 7.6        |
| $\Delta \kappa_\gamma \cdot 10^{-04}$  | 6.4          | 7.7        |
| $\Delta \lambda_\gamma \cdot 10^{-04}$ | 7.2          | 15.5       |

Table 8: Summary of the results obtained with the simultaneous fit of polarization and TGCs for a total luminosity of  $500 \text{ fb}^{-1}$  and for two different choices of the binning. A binning of 10-5-5 (20-10-10) is intended as respectively 20 (10), 10 (5) and 10 (5) bins for the  $\cos \theta_W$ ,  $\cos \theta_i^*$  and  $\phi_i^*$  distributions.

| Parameters                     | 60% $P_{e^+}$ | 30% $P_{e^+}$ |
|--------------------------------|---------------|---------------|
| $P_{e^-}/P_{e^+}$              | 13.3          | -2.7          |
| $P_{e^-}/g_1^Z$                | -0.8          | 9.1           |
| $P_{e^-}/\kappa_\gamma$        | -12.8         | -15.3         |
| $P_{e^-}/\lambda_\gamma$       | 4.3           | -6.1          |
| $P_{e^+}/g_1^Z$                | 2.8           | 0.2           |
| $P_{e^+}/\kappa_\gamma$        | -7.4          | -9.5          |
| $P_{e^+}/\lambda_\gamma$       | -6.3          | -2.5          |
| $g_1^Z/\kappa_\gamma$          | 70.2          | 63.4          |
| $g_1^Z/\lambda_\gamma$         | 47.1          | 47.7          |
| $\lambda_\gamma/\kappa_\gamma$ | 47.2          | 35.4          |

Table 9: Correlations between the fit parameters obtained with the angular fit of polarization and TGCs. The results for both the options of 60% and 30% positron polarization are reported.

## 7 Systematics

In this section the main sources of systematics that might affect the polarization and the TGCs measurements at the future ILC are investigated. In particular, the assumption made so far that reversing the sign of the polarization does not affect its absolute value is studied in detail.

### 7.0.1 Efficiency

The measurements implemented make use of non-normalized distributions, therefore a correct evaluation of the selection efficiency is a key factor. At LEP [25] uncertainties on the selection efficiencies of the order of  $\sim 0.1\%$  have been obtained, for the semileptonic decays of the  $W$ -pairs. In order to be conservative, an error of  $0.2\%$  on the selection efficiency of signal and tau-signal has been considered (note that the statistical error on the selection efficiencies in Tab. 3 refers to just  $20 \text{ fb}^{-1}$  of statistics. For the higher considered luminosities, in particular for a total luminosity of  $500 \text{ fb}^{-1}$ , the statistical error on the selection efficiency is negligible and is expected to be limited by systematic effects). Uncertainties on the selection efficiency of the background of  $1\%$  and  $5\%$  have been considered. These uncertainty have been propagated as a global rescaling of the background. The case of an error of  $0.5\%$  on the selection efficiency of the signal and of the tau-signal has also been considered.

The impact on the measurement of polarization and TGCs is summarized in Tables 10 and 11, respectively for the low and high positron polarization options. If the selection efficiency of the signal can be controlled with a precision of at least  $0.2\%$  the measurements are robust with regard to this source of systematics. Uncertainties of the order of  $0.5\%$  would limit the statistical precision on the TGCs at high luminosities, though at the  $10^{-3}$  level, which would still be one order of magnitude better than the limits obtained at LEP. The measurement of the polarization is found to be reasonably robust with regard to this source of systematics. Even with the most conservative assumptions the propagation of the uncertainty to the measurement of the polarization does not exceed the statistical uncertainty for an integrated luminosity of  $500 \text{ fb}^{-1}$ .

### 7.0.2 Integrated Luminosity

A relative accuracy better than  $10^{-3}$  on the integrated luminosity is needed at the ILC in order to achieve the physics goals [1]. An error of the order of  $10^{-3}$  was achieved in preliminary simulation studies using Bhabha events [26]. Some of the uncertainties contributing to this error could still be improved, like the large uncertainty coming from the two-photon background, that can be reduced correcting for it and instead using the uncertainty from higher order simulations as a true source of systematics on the luminosity measurement [26].

The biggest impact on the polarization and TGCs measurement coming from this source of systematic error is obtained in case it influences the four polarization sets  $++$ ,  $+-$ ,  $-+$  and  $--$  differently, namely increasing the integrated luminosity of some samples with respect to the nominal value, while reducing it for others. Using fast helicity flipping also for the positron beam, this eventuality can most probably be warded off. The maximum impact of a  $10^{-3}$  error on the integrated luminosity to the polarization and TGCs measurements is shown in Tab. 12. It is found that this source of systematics does not limit

| Parameter                 | Blondel | Angular no TGCs | Angular with TGCs |
|---------------------------|---------|-----------------|-------------------|
| 0.2% signal 1% background |         |                 |                   |
| $\Delta P_{e^+}$          | 0.03%   | 0.01%           | 0.01%             |
| $\Delta P_{e^-}$          | 0.02%   | 0.01%           | 0.01%             |
| $\Delta g_1^Z$            | -       | -               | 0.0006            |
| $\Delta \kappa_\gamma$    | -       | -               | 0.0007            |
| $\Delta \lambda_\gamma$   | -       | -               | 0.00002           |
| 0.2% signal 5% background |         |                 |                   |
| $\Delta P_{e^+}$          | 0.08%   | 0.05%           | 0.05%             |
| $\Delta P_{e^-}$          | 0.07%   | 0.05%           | 0.05%             |
| $\Delta g_1^Z$            | -       | -               | 0.001             |
| $\Delta \kappa_\gamma$    | -       | -               | 0.001             |
| $\Delta \lambda_\gamma$   | -       | -               | 0.0007            |
| 0.5% signal 1% background |         |                 |                   |
| $\Delta P_{e^+}$          | 0.04%   | 0.01%           | 0.01%             |
| $\Delta P_{e^-}$          | 0.03%   | 0.01%           | 0.01%             |
| $\Delta g_1^Z$            | -       | -               | 0.001             |
| $\Delta \kappa_\gamma$    | -       | -               | 0.001             |
| $\Delta \lambda_\gamma$   | -       | -               | 0.0004            |
| 0.5% signal 5% background |         |                 |                   |
| $\Delta P_{e^+}$          | 0.08%   | 0.05%           | 0.05%             |
| $\Delta P_{e^-}$          | 0.07%   | 0.05%           | 0.06%             |
| $\Delta g_1^Z$            | -       | -               | 0.002             |
| $\Delta \kappa_\gamma$    | -       | -               | 0.002             |
| $\Delta \lambda_\gamma$   | -       | -               | 0.0008            |

Table 10: *Summary of the systematics due to the uncertainties on the selection efficiencies, for the low positron polarization option of 30%. The impact on the polarization and TGCs measurement is shown, both for the Blondel technique and for the angular fit method.*

| Parameter                 | Blondel | Angular no TGCs | Angular with TGCs |
|---------------------------|---------|-----------------|-------------------|
| 0.2% signal 1% background |         |                 |                   |
| $\Delta P_{e^+}$          | 0.02%   | 0.01%           | 0.01%             |
| $\Delta P_{e^-}$          | 0.03%   | 0.01%           | 0.01%             |
| $\Delta g_1^Z$            | -       | -               | 0.0006            |
| $\Delta \kappa_\gamma$    | -       | -               | 0.0006            |
| $\Delta \lambda_\gamma$   | -       | -               | 0.0002            |
| 0.2% signal 5% background |         |                 |                   |
| $\Delta P_{e^+}$          | 0.08%   | 0.05%           | 0.05%             |
| $\Delta P_{e^-}$          | 0.07%   | 0.05%           | 0.05%             |
| $\Delta g_1^Z$            | -       | -               | 0.001             |
| $\Delta \kappa_\gamma$    | -       | -               | 0.002             |
| $\Delta \lambda_\gamma$   | -       | -               | 0.0006            |
| 0.5% signal 1% background |         |                 |                   |
| $\Delta P_{e^+}$          | 0.03%   | 0.01%           | 0.01%             |
| $\Delta P_{e^-}$          | 0.03%   | 0.01%           | 0.01%             |
| $\Delta g_1^Z$            | -       | -               | 0.001             |
| $\Delta \kappa_\gamma$    | -       | -               | 0.001             |
| $\Delta \lambda_\gamma$   | -       | -               | 0.0002            |
| 0.5% signal 5% background |         |                 |                   |
| $\Delta P_{e^+}$          | 0.08%   | 0.05%           | 0.05%             |
| $\Delta P_{e^-}$          | 0.07%   | 0.05%           | 0.05%             |
| $\Delta g_1^Z$            | -       | -               | 0.002             |
| $\Delta \kappa_\gamma$    | -       | -               | 0.002             |
| $\Delta \lambda_\gamma$   | -       | -               | 0.0008            |

Table 11: *Summary of the systematics from the selection efficiencies, for the high positron polarization option of 60%. The impact on the polarization and TGCs measurement is shown, both for the Blondel technique and for the angular fit method.*

| Parameter                              | Blondel | Angular no TGCs | Angular with TGCs |
|--|---------|-----------------|-------------------|
| 60% $e^+$ polarization                 |         |                 |                   |
| $\Delta P_{e^+}$                       | 0.1%    | 0.08%           | 0.07%             |
| $\Delta P_{e^-}$                       | 0.04%   | 0.02%           | 0.02%             |
| $\Delta g_1^Z \cdot 10^{-04}$          | -       | -               | 0.0002            |
| $\Delta \kappa_\gamma \cdot 10^{-04}$  | -       | -               | 0.0002            |
| $\Delta \lambda_\gamma \cdot 10^{-04}$ | -       | -               | 0.0002            |
| 30% $e^+$ polarization                 |         |                 |                   |
| $\Delta P_{e^+}$                       | 0.3%    | 0.2%            | 0.2%              |
| $\Delta P_{e^-}$                       | 0.08%   | 0.03%           | 0.02%             |
| $\Delta g_1^Z \cdot 10^{-04}$          | -       | -               | 0.0002            |
| $\Delta \kappa_\gamma \cdot 10^{-04}$  | -       | -               | 0.0002            |
| $\Delta \lambda_\gamma \cdot 10^{-04}$ | -       | -               | 0.0001            |

Table 12: Maximum impact of the luminosity uncertainty on the measurement of polarization and TGCs. An error of  $10^{-3}$  on the integrated luminosity was assumed.

|                                   | 30% $P_{e^+}$ | 60% $P_{e^+}$ |
|-----------------------------------|---------------|---------------|
| $\Delta P_{e^+}^+ / P_{e^+}^+ \%$ | 8.04          | 3.87          |
| $\Delta P_{e^+}^- / P_{e^+}^- \%$ | 4.06          | 0.94          |
| $\Delta P_{e^-}^+ / P_{e^-}^+ \%$ | 0.44          | 0.34          |
| $\Delta P_{e^-}^- / P_{e^-}^- \%$ | 4.04          | 3.22          |
| corr $P_{e^+}^+ P_{e^-}^+ \%$     | 97.8          | 96.9          |
| corr $P_{e^+}^+ P_{e^-}^- \%$     | 99.7          | 99.6          |
| corr $P_{e^+}^- P_{e^-}^+ \%$     | 95.8          | 95.7          |
| corr $P_{e^+}^- P_{e^-}^- \%$     | 99.2          | 98.6          |

Table 13: Summary of the results obtained with the angular fit method, without making the assumption that the absolute value of the polarization remains unchanged, when flipping its sign. The total luminosity of  $500 \text{ fb}^{-1}$  is equally shared between the four polarization sets.

significantly the statistical precision obtained for an integrated luminosity of  $500 \text{ fb}^{-1}$ , both for the polarization and the TGCs measurements.

### 7.0.3 Assumptions on the Polarization

So far it was assumed that the left-handed and the right-handed states of the polarizations have the same magnitude. In order to make realistic estimates of the precisions achievable at the ILC this constraint needs to be checked. This assumption is in principle not necessary in the angular fit method, unlike the Blondel scheme. The fit of the polarizations can be executed using two different parameters for the different signs of the polarizations. However, this leads to a dramatic worsening of the statistical precision. The results obtained for a total luminosity of  $500 \text{ fb}^{-1}$  are summarized in Tab. 13. The luminosity is assumed to be equally shared between the four polarization sets. The precision obtained is well above the desired 0.2% and the correlation between the fit parameters is very high.

It is possible to repeat the measurement with different assumptions, taking into account

the additional information given by the polarimeters. This possibility has been addressed for the most precise technique implemented, the angular fit method, both with and without additional measurement of the TGCs.

At the ILC, the polarization will be measured by the polarimeters with an expected uncertainty of  $\sim \Delta P/P = 0.25\%$  [27]. Preliminary spin tracking studies, based on the ILC RDR lattice and beam parameter set, show that the depolarization between the polarimeters and the IP is the same for the two helicity states of the same beam, with negligible residual differences<sup>a</sup>. Therefore, the 4 average luminosity-weighted polarizations at the IP  $P_{e^+}^+$ ,  $P_{e^+}^-$ ,  $P_{e^-}^+$  and  $P_{e^-}^-$  can be constrained as follows:

$$\begin{aligned} P_+ &= \frac{P_{e^+}^+ + P_{e^+}^-}{2}, \\ \epsilon_+ &= \frac{P_{e^+}^+ - P_{e^+}^-}{2}, \\ P_- &= \frac{P_{e^-}^+ + P_{e^-}^-}{2}, \\ \epsilon_- &= \frac{P_{e^-}^+ - P_{e^-}^-}{2}, \end{aligned} \tag{29}$$

where  $P_{e^+}^-$  ( $P_{e^-}^-$ ) and  $P_{e^+}^+$  ( $P_{e^-}^+$ ) are the magnitudes of the positron (electron) polarization in the left-handed and in the right-handed state, respectively, as measured by the polarimeters.

When performing the angular fit, one free parameter for the polarization of each beam is used,  $par_+$  for the positron beam and  $par_-$  for the electron beam. In the data samples where the positron is right-handed, the positron polarization is fitted with:

$$par_+ + \epsilon_+, \tag{30}$$

while the left-handed state is fitted with:

$$-par_+ + \epsilon_+. \tag{31}$$

The same equations hold for the polarization of the electron beam. The performance of the fit is not affected by the value of  $\epsilon_{\pm}$ , what matters is the precision with which it can be determined, which is:

$$\sigma_{\epsilon_{\pm}} \approx \frac{0.0025 P_{\pm}}{\sqrt{2}}, \tag{32}$$

where  $P_{\pm}$  was defined in Eq. 29. In order to take this uncertainty into account, for each iteration of the fit  $\epsilon_{\pm}$  is smeared randomly using a Gaussian with a width of  $\sigma_{\epsilon_{\pm}}$ . This smearing is performed in addition to the Poissonian smearing of the data samples for each iteration of the fit. For simplicity this version of the fit will be called in the following *realistic*, as opposed to the *idealistic* fit, where  $|P_{e^+}^-| = |P_{e^+}^+|$  and  $|P_{e^-}^-| = |P_{e^-}^+|$ .

The two modalities of the fit are compared in Fig. 27 and Tab. 14. The dependence of the obtained precisions on the total luminosity is shown in Fig. 27. For a total luminosity

---

<sup>a</sup>Moritz Beckmann, private communication.

| $e^+$ pol  | $\Delta P_{e^+}/P_{e^+}\%$ | $\Delta P_{e^-}/P_{e^-}\%$ | corr $^{\circ}\%$ |
|------------|----------------------------|----------------------------|-------------------|
| Idealistic |                            |                            |                   |
| 30         | 0.34                       | 0.08                       | 6.6               |
| 60         | 0.14                       | 0.08                       | 3.4               |
| Realistic  |                            |                            |                   |
| 30         | 0.35                       | 0.16                       | -3.7              |
| 60         | 0.17                       | 0.16                       | -5.9              |

Table 14: Summary of the results obtained with the angular fit method for a total luminosity of  $500 \text{ fb}^{-1}$ . The idealistic case is compared with the realistic case, which takes into account the polarimeters measurement, with a 0.25% uncertainty. The numbers refer to an electron polarization of 80%. The results for both the options of 30% and 60% positron polarization are shown.

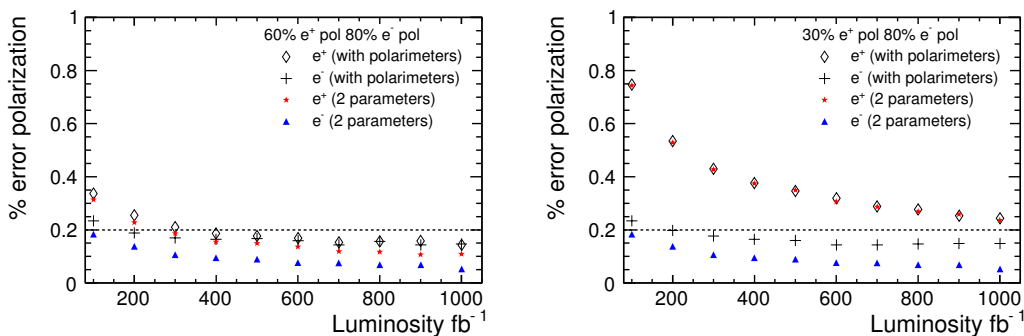


Figure 27: Summary of the results obtained with the angular fit method. The idealistic case is compared with the realistic case, which takes into account the polarimeters measurement, with a 0.25% uncertainty. The distribution on the left (right) refers to a positron polarization of 60% (30%). The simultaneous fit of polarization and TGCs has been performed using the log-likelihood technique and a binning of respectively 10, 5 and 5 bins for the  $\cos\theta_W$ ,  $\cos\theta_t^*$  and  $\phi_t^*$  distributions.

of  $500 \text{ fb}^{-1}$  the error is essentially dominated by the systematic uncertainty from the  $\pm$  polarization differences, when considering the 60% positron polarization option. In the 30% polarization option, improvements at higher luminosities can be obtained for the positron polarization, due to the lower statistical precision. Considering that this is a result realistically achievable at the ILC, it is fully satisfactory. Precisions better than 0.2% can be obtained on the electron polarization and on the positron polarization, if a high positron polarization is considered. In the case of 30% positron polarization, the effect of the uncertainty on the measurement of the positron polarization is negligible, since the polarization has a worse statistical precision.

When moving from the idealistic to the realistic assumptions in the simultaneous measurement of TGCs and polarization, no significant impact on the TGCs measurement is found. The results are compared in Tab. 15. The sensitivity to the couplings is comparable to the sensitivity obtained with the idealistic assumptions, while the sensitivity to the po-

| Parameter                              | Realistic | Idealistic |
|--|-----------|------------|
| 60% $P_{e^+}$                          |           |            |
| $\Delta P_{e^+} \%$                    | 0.17      | 0.14       |
| $\Delta P_{e^-} \%$                    | 0.16      | 0.09       |
| $\Delta g_1^Z \cdot 10^{-04}$          | 7.7       | 7.3        |
| $\Delta \kappa_\gamma \cdot 10^{-04}$  | 7.9       | 7.4        |
| $\Delta \lambda_\gamma \cdot 10^{-04}$ | 15.2      | 15.3       |
| 30% $P_{e^+}$                          |           |            |
| $\Delta P_{e^+} \%$                    | 0.35      | 0.34       |
| $\Delta P_{e^-} \%$                    | 0.16      | 0.08       |
| $\Delta g_1^Z \cdot 10^{-04}$          | 7.9       | 7.6        |
| $\Delta \kappa_\gamma \cdot 10^{-04}$  | 7.6       | 7.7        |
| $\Delta \lambda_\gamma \cdot 10^{-04}$ | 15.6      | 15.5       |

Table 15: Summary of the results obtained for the angular fit of polarization and TGCs for a total luminosity of  $500 \text{ fb}^{-1}$  and with a binning of 10-5-5. The realistic and the idealistic fits are compared.

larization is comparable to the one obtained with the realistic fit of the polarization only. The correlations between couplings and polarization are summarized in Tab. 16 and are acceptable.

## 8 Conclusions

Using the  $W$ -pair production it will be possible to measure the average luminosity-weighted beam polarization at the ILC with high sensitivity, providing the polarimeters with an absolute scale calibration.

Applying a modified Blondel scheme, a statistical uncertainty of 0.1% (0.2%) on the  $e^-$  ( $e^+$ ) polarization is obtained for an integrated luminosity of  $\mathcal{L} = 500 \text{ fb}^{-1}$ , an electron polarization of 80% and for a high positron polarization of 60%. When considering the lower positron polarization option of 30%, the measurement precision reduces to 0.2% (0.5%) for the  $e^-$  ( $e^+$ ) polarization.

Using an angular fit technique, which compares the distribution of the production angle of the  $W$ -pair to a Monte Carlo template, the same precision on the polarization is obtained already for lower luminosities. This method requires a total luminosity of only  $250 \text{ fb}^{-1}$  for the high positron polarization option, in order to achieve a statistical precision of the order of 0.1% (0.2%) on the polarization of the electron (positron) beam. For the lower positron polarization option a precision of 0.1% (0.34%) on the  $e^-$  ( $e^+$ ) polarization is obtained for an integrated luminosity of  $\mathcal{L} = 500 \text{ fb}^{-1}$ .

Since the angular fit method require lower luminosities, it also allows a reduction of the luminosity spent with both beams right-handed or left-handed. Such configurations of the helicities are of low interest for most of the physics studies, since they suppress the  $s$ -channel diagrams. With the angular fit method, only 20% of the total luminosity need to be spent on these polarization configurations to obtain a statistical precision of the order of 0.1% (0.2%) on the polarization of the  $e^-$  ( $e^+$ ) beam for an integrated luminosity of  $400 \text{ fb}^{-1}$ .

| Parameters                     | 60% $P_{e^+}$ | 30% $P_{e^+}$ |
|--------------------------------|---------------|---------------|
| $P_{e^-}/P_{e^+}$              | -2.9          | -1.7          |
| $P_{e^-}/g_1^Z$                | 32.2          | 35.6          |
| $P_{e^-}/\kappa_\gamma$        | 28.6          | 26.0          |
| $P_{e^-}/\lambda_\gamma$       | 3.3           | 4.8           |
| $P_{e^+}/g_1^Z$                | 20.3          | 7.2           |
| $P_{e^+}/\kappa_\gamma$        | 13.9          | 3.1           |
| $P_{e^+}/\lambda_\gamma$       | 3.1           | -0.1          |
| $g_1^Z/\kappa_\gamma$          | 72.2          | 70.1          |
| $g_1^Z/\lambda_\gamma$         | 38.6          | 41.0          |
| $\lambda_\gamma/\kappa_\gamma$ | 37.3          | 38.5          |

Table 16: Correlations between the fit parameters obtained with the angular fit of polarization and TGCs, in both the options of 60% and 30% positron polarization. The results shown were obtained with the realistic fit.

The angular fit method can be extended to a simultaneous fit of polarization and TGCs without losing sensitivity on the polarization. Three independent couplings in the vertices  $WW\gamma$  and  $WWZ$  were fitted together with the polarization, obtaining an absolute statistical precision better than  $10^{-3}$  for an integrated luminosity of  $\mathcal{L} = 500 \text{ fb}^{-1}$ .

A study of the possible systematic errors that might affect the performance of the measurement has been performed. The major effect comes from differences in the values of the left- and right-handed states of the polarizations, that need to be corrected using the polarimeters. Propagating the expected 0.25% uncertainty of the polarimeters, the impact on the polarization and TGCs measurement has been evaluated. While no significant impact on the TGCs measurement is found, the systematic uncertainty on the polarization is non-negligible and dominates over the statistical precision at high luminosities. However, good precisions are achieved even considering this source of systematics. For a high positron polarization of 60%, an uncertainty of 0.16% (0.17%) for the  $e^-$  ( $e^+$ ) polarization is obtained for an integrated luminosity of  $\mathcal{L} = 500 \text{ fb}^{-1}$ . Assuming a lower positron polarization of 30%, the achieved precision is 0.16% (0.35%) for the  $e^-$  ( $e^+$ ) polarization.

## Acknowledgments

This work profited from several discussions with Mikael Berggren and Jenny List.

We would like to thank the DESY simulation production team, in particular Steve Aplin, Jan Engels and Andreas Gellrich, for their great effort in contributing to produce the large samples of Monte Carlo events used in this work.

We would like to thank Jörgen Samson, for the support and for his advice about the event generators and Whizard, and Jadranka Sekaric, for sharing her experience in simulating the TGCs.

We are grateful to Daniela Käfer for proof reading most of the note.

We acknowledge the support of the DFG through the SFB (grant SFB 676/1-2006).

## List of Figures

|    |   |    |
|----|---|----|
| 1  | Total cross section of the $W$ -pair production measured at LEP . . . . . | 4  |
| 2  | Fit results on the triple gauge couplings at LEP . . . . .                | 6  |
| 3  | Polarization configurations in $s$ -channel diagrams . . . . .            | 8  |
| 4  | Polarization configurations in crossed channels . . . . .                 | 8  |
| 5  | Leading tree-level Feynman diagrams for the $W^+W^-$ production . . . . . | 9  |
| 6  | Total cross section of the $W$ -pair production . . . . .                 | 10 |
| 7  | Preselection . . . . .  | 13 |
| 8  | Jet finder $y$ variables . . . . .  | 14 |
| 9  | Isolation and tau-signal exclusion . . . . .                              | 15 |
| 10 | Initial state radiation correction . . . . .                              | 16 |
| 11 | Invariant mass and invariant mass resolution . . . . .                    | 17 |
| 12 | Distribution of $\cos\theta_W$ . . . . .                                  | 17 |
| 13 | Results of the Blondel scheme . . . . .                                   | 20 |
| 14 | Templates of $\cos\theta_W$ : discrete distributions . . . . .            | 21 |
| 15 | Templates of $\cos\theta_W$ : fit . . . . .                               | 23 |
| 16 | Angular fit: distributions of the fitted parameters . . . . .             | 24 |
| 17 | Angular fit: fit probability . . . . .                                    | 25 |
| 18 | Blondel versus angular fit . . . . .                                      | 26 |
| 19 | Reducing the $++$ and $--$ helicity combinations . . . . .                | 26 |
| 20 | Topology of the $W$ -pair . . . . .                                       | 30 |
| 21 | Leptonic decay angles of the $W$ -pair and their resolution . . . . .     | 31 |
| 22 | Impact of the TGCs on the angular distributions . . . . .                 | 32 |
| 23 | Binning issues for the angular fit . . . . .                              | 34 |
| 24 | Checks based on the $\chi^2$ . . . . .                                    | 36 |
| 25 | Results for the angular fit with and without TGCs measurement . . . . .   | 36 |
| 26 | Uncertainty on the TGCs . . . . .   | 37 |
| 27 | Results for the angular fit: realistic versus idealistic . . . . .        | 44 |

## List of Tables

|    |   |    |
|----|---|----|
| 1  | <i>WW</i> decay modes and relative selection efficiencies at LEP . . . . .  | 5  |
| 2  | Number of signal and background events before the selection . . . . .   | 12 |
| 3  | Selection flow . . . . .  | 18 |
| 4  | Summary of the angular fit results with 2 free parameters . . . . .   | 25 |
| 5  | Sets of TGCs used to calculate the coefficients of $R(\Delta g_1^Z, \Delta \kappa_\gamma, \Delta \lambda_\gamma)$ . . . . . | 27 |
| 6  | Measurement of the TGCs at LEP . . . . .  | 28 |
| 7  | Uncertainty on the TGCs propagated to the polarization measurement . . . . .  | 29 |
| 8  | Results of the simultaneous measurement of TGCs and polarization . . . . .  | 38 |
| 9  | Correlations in the simultaneous measurement of TGCs and polarization . . . . .   | 38 |
| 10 | Systematics on the selection efficiencies: low positron polarization . . . . .  | 40 |
| 11 | Systematics on the selection efficiencies: high positron polarization . . . . .   | 41 |
| 12 | Systematics on the integrated luminosity . . . . .  | 42 |
| 13 | Summary of the angular fit results with 4 free parameters . . . . .   | 42 |
| 14 | Summary of the angular fit results including polarimeters . . . . .   | 44 |
| 15 | TGCs and polarization measurement: realistic versus idealistic . . . . .  | 45 |
| 16 | Correlations in the realistic measurement of TGCs and polarization . . . . .  | 46 |

## References

- [1] T. Abe *et al.*, “The International Large Detector: Letter of Intent,” 2010.
- [2] J. Sekaric, “Studies of gauge boson production with a  $\gamma\gamma$  collider at TESLA,” 2005.
- [3] G. Abbiendi *et al.*, “ $W^+W^-$  production and triple gauge boson couplings at LEP energies up to 183-GeV,” *Eur. Phys. J.*, vol. C8, pp. 191–215, 1999.
- [4] P. Spagnolo, “Boson gauge couplings at LEP,” 2005.
- [5] W. Buchmuller and D. Wyler, “Effective Lagrangian Analysis of New Interactions and Flavor Conservation,” *Nucl. Phys.*, vol. B268, p. 621, 1986.
- [6] G. Gounaris *et al.*, “Triple gauge boson couplings,” 1996.
- [7] H. Aronson, “Spin-1 electrodynamics with an electric quadrupole moment,” *Phys. Rev.*, vol. 186, pp. 1434–1441, 1969.
- [8] T. L. C. ALEPH, DELPHI, L3, OPAL, and the LEP TGC Working Group, “A combination of results on charged triple gauge boson couplings measured by the LEP experiments,” LEPEWWG/TGC/2005-01.
- [9] P. Achard *et al.*, “Production of single  $W$  bosons at LEP and measurement of  $WW\gamma$  gauge coupling parameters,” *Phys. Lett.*, vol. B547, pp. 151–163, 2002.
- [10] S. Schael *et al.*, “Single vector boson production in  $e^+e^-$  collisions at centre-of-mass energies from 183 GeV to 209 GeV,” *Phys. Lett.*, vol. B605, pp. 49–62, 2005.
- [11] A. Heister *et al.*, “Single photon and multiphoton production in  $e^+e^-$  collisions at  $\sqrt{s}$  up to 209 GeV,” *Eur. Phys. J.*, vol. C28, pp. 1–13, 2003.
- [12] P. Achard *et al.*, “Single photon and multiphoton events with missing energy in  $e^+e^-$  collisions at LEP,” *Phys. Lett.*, vol. B587, pp. 16–32, 2004.
- [13] K. J. F. Gaemers and G. J. Gounaris, “Polarization Amplitudes for  $e^+e^- \rightarrow W^+W^-$  and  $e^+e^- \rightarrow ZZ$ ,” *Zeit. Phys.*, vol. C1, p. 259, 1979.
- [14] S. Schael *et al.*, “Improved measurement of the triple gauge-boson couplings  $\gamma WW$  and  $ZWW$  in  $e^+e^-$  collisions,” *Phys. Lett.*, vol. B614, pp. 7–26, 2005.
- [15] V. M. Abazov *et al.*, “Measurement of the  $WZ \rightarrow \ell\nu\ell\ell$  cross section and limits on anomalous triple gauge couplings in  $p\bar{p}$  collisions at  $\sqrt{s} = 1.96$  TeV,” *Phys. Lett.*, vol. B695, pp. 67–73, 2011.
- [16] T. Aaltonen *et al.*, “Limits on Anomalous Triple Gauge Couplings in  $p\bar{p}$  Collisions at  $\sqrt{s} = 1.96$  TeV,” *Phys. Rev.*, vol. D76, p. 111103, 2007.
- [17] G. Aad *et al.*, “Expected Performance of the ATLAS Experiment - Detector, Trigger and Physics,” 2009.
- [18] G. A. Moortgat-Pick *et al.*, “The role of polarized positrons and electrons in revealing fundamental interactions at the linear collider,” *Phys. Rept.*, vol. 460, pp. 131–243, 2008.
- [19] G. Abbiendi *et al.*, “Measurement of the  $e^+e^- \rightarrow W^+W^-$  cross section and  $W$  decay branching fractions at LEP,” *Eur. Phys. J.*, vol. C52, pp. 767–785, 2007.
- [20] Y. L. Dokshitzer, G. D. Leder, S. Moretti, and B. R. Webber, “Better jet clustering algorithms,” *JHEP*, vol. 08, p. 001, 1997.
- [21] A. Blondel, “A Scheme to measure the polarization asymmetry at the  $Z$  pole in LEP,” *Phys. Lett.*, vol. B202, p. 145, 1988.
- [22] K. Mönig, “The use of positron polarization for precision measurements,” LC-PHSM-2000-059.
- [23] F. James and M. Roos, “Minuit: A System for Function Minimization and Analysis of the Parameter Errors and Correlations,” *Comput. Phys. Commun.*, vol. 10, pp. 343–367, 1975.
- [24] R. J. Barlow and C. Beeston, “Fitting using finite Monte Carlo samples,” *Comput. Phys. Commun.*, vol. 77, pp. 219–228, 1993.
- [25] A. Heister *et al.*, “Measurement of  $W$  pair production in  $e^+e^-$  collisions at centre-of-mass energies from 183 GeV to 209 GeV,” *Eur. Phys. J.*, vol. C38, pp. 147–160, 2004.
- [26] I. Bozovic-Jelisavcic *et al.*, “Luminosity Measurement at ILC,” 2010.
- [27] S. Boogert *et al.*, “Polarimeters and Energy Spectrometers for the ILC Beam Delivery System,” *JINST*, vol. 4, p. P10015, 2009.